Title

Characterization of the contractile properties of primary human trabecular meshwork cells at the single-cell level

Author

Sanchez, Luis Uriel

Publication Date

2023

Peer reviewed|Thesis/dissertation

UNIVERSITY OF CALIFORNIA

Los Angeles

Characterization of the contractile properties of primary human trabecular meshwork cells at the single-cell level

A dissertation submitted in partial satisfaction of the

requirements for the degree of Doctor of Philosophy

in Molecular Biology

by

Luis Uriel Sanchez

2023

ABSTRACT OF THE DISSERTATION

Characterization of the contractile properties of primary human trabecular meshwork cells at the single-cell level

by

Luis Uriel Sanchez

Doctor of Philosophy in Molecular Biology

University of California, Los Angeles, 2023

Professor Jie J. Zheng, Chair

Steroid induced ocular hypertension is a serious adverse effect of prolonged steroid therapy in patients. If left untreated, steroid induced ocular hypertension may progress to steroid induced glaucoma, involving glaucomatous optic neuropathy and permanent vision loss. Chronic steroid administration elevates intraocular pressure in approximately 40% of the general population. If this increase is of sufficient magnitude and duration, steroid induced ocular hypertension may develop. This condition is associated with the abnormal contractility of the cells residing within the trabecular meshwork, the tissue responsible for intraocular pressure regulation. Numerous studies have provided insight into the molecular mechanism changes that occur in the trabecular meshwork as a result of prolonged steroid exposure. These changes include but are not limited to alterations in extracellular matrix metabolism, cytoskeletal organization, and gene expression. However, the specific functional changes occurring at the cellular level as a result of these molecular alterations, which contribute to trabecular meshwork dysfunction and ultimately ocular hypertension, remain poorly characterized. To address the need for a comprehensive evaluation of contractile cell function, we have adapted and optimized an assay, hereinafter referred to as

fluorescently labeled elastomeric contractible surfaces (FLECS), to assess the functional effects of steroids on human trabecular meshwork cells *in vitro*. The FLECS assay provides a flexible tool for obtaining contractility measurements of thousands of cells at the single-cell level on substrates with tunable stiffness. In this thesis, I present, for the first time, single-cell-level contractile variations in human trabecular meshwork cells in primary culture and in an *in vitro* model of chronic steroid exposure. Furthermore, I report alterations in single-cell contraction kinetics associated with modifications in extracellular matrix substrates and stiffness, as well as the addition of a ROCK inhibitor. These findings provide compelling supportive evidence for a model in which increased contractility, accompanied by changes in extracellular matrix components, cytoskeletal organization, and stiffness, may contribute to elevated intraocular pressure and, consequently, ocular hypertension.

The dissertation of Luis Uriel Sanchez is approved.

Roxana Radu

Gregory S. Payne

Alex Huang

Jie J. Zheng, Committee Chair

University of California, Los Angeles

2023

This dissertation is dedicated to

My loving family, through thick and thin.

TABLE OF CONTENTS

VITA

EDUCATION

University of California, Los Angeles 2016

Ph.D. Candidate, Molecular Biology (Cell and Developmental Biology)

San Francisco State University 2015

B.S., Cell and Molecular Biology

RESEARCH EXPERIENCE

University of California, Los Angeles 2016-Present

Graduate Student Researcher; Advisor: Jie J. Zheng, Ph.D.

Eureka Therapeutics, Inc. 2015-2016

Research Associate

San Francisco State University 2014-2015

Undergraduate Student Researcher; Advisor: Laura W. Burrus, Ph.D.

PUBLICATIONS

Graybeal, K, **Sanchez, L.**, Zhang, C, Stiles, L, Zheng, JJ. Characterizing the metabolic profile of dexamethasone treated human trabecular meshwork cells. *Experimental Eye Research* (2022).

Galli, LM, Anderson, MO, Fraley, JG, **Sanchez, L**, Bueno, R, Hernandez, DN, Maddox, EU, Lingappa, VR, and Burrus, LW. Determination of the membrane topology of PORCN, an O-acyl transferase that modifies Wnt signaling proteins. *Open Biology* (2021).

SELECTED HONORS AND AWARDS

T32 Vision Training Grant	2020-2022
Vision Health Research Network Travel Award	2022
International Society for Eye Research Travel Award	2022
NIH-NIGMS Diversity Supplement Award	2017-2018
MBRS-RISE Fellowship Award	2014-2015
NIH-MARC Honors Program	2014-2015
IRA Grant for Student Research in Biology	2014-2015
NSF Research Experience for Undergraduate Students	2014
Louis Stokes Alliance for Minority Participation Fellowship	2014

SEMINARS AND POSTER PRESENTATIONS

Single-cell variations in the contractility of human trabecular meshwork cells. Department of Ophthalmology Annual Vision Science Retreat. UCLA, CA. November 2023.

Human trabecular meshwork (HTM) cell isolation, culture, and contractile property characterization. Department of Ophthalmology Annual Vision Science Retreat. Lake Arrowhead, CA. October 2022.

Time-course analysis of human trabecular meshwork single-cell contraction after a 5-day dexamethasone treatment. Vision Restoration Summer School. Quebec, Canada. July 2022.

Time-course analysis of human trabecular meshwork single-cell contraction after a 5-day dexamethasone treatment. ISER/Bright Focus Glaucoma Symposium. Atlanta, GA. May 2022.

Chapter 1: Introduction

Aqueous humor dynamics

Aqueous humor is a fluid-like substance that fills the eye's anterior and posterior segments and is critical for its structure and function. It is composed of a complex mixture of electrolytes, organic solutes, growth factors, cytokines, and other proteins[1]. This transparent water-like fluid, similar to blood plasma, nourishes the avascular tissues of the anterior segment, removes waste products (e.g., metabolic & cellular debris), and maintains the shape as well as the optical properties of the eye. Additionally, aqueous humor facilitates the circulation of inflammatory cells and their mediators during pathological conditions and enables the distribution of drugs to various ocular structures[2,3,4,5].

The process of aqueous humor production and circulation in the eye begins with the inflow of blood into the ciliary body from the posterior ciliary arteries[6]. Aqueous humor is then secreted by the nonpigmented epithelium of the ciliary body at a rate of approximately 2-3 μL/min by the processes of ultrafiltration, simple diffusion, and active secretion into the posterior chamber. From the posterior chamber, aqueous humor flows between the lens and iris into the anterior chamber. Once it has entered the anterior chamber, aqueous humor may leave the eye via 2 pathways known as the unconventional, and the conventional outflow pathways, with the former being mostly pressure insensitive and the latter being pressure sensitive. In the unconventional outflow pathway, a fraction of aqueous humor passes through the posterior-most aspect of the uveal meshwork and the anterior surface of the ciliary muscle. Aqueous humor then enters the interstitial spaces between the longitudinal ciliary muscle bundles and into the supraciliary and the suprachoroidal spaces, where it enters the sclera or is absorbed by the choroid[7]. In the conventional outflow pathway, aqueous humor passes through the trabecular meshwork into the Schlemm's canal, flows into the collector channels, and then enters the episcleral venous system

where it re-enters the systemic cardiovascular circulation, completing the cycle[8]. While present, the unconventional outflow pathway has significantly less impact on intraocular pressure and is considered a secondary route for aqueous humor drainage. Instead, the conventional outflow pathway is recognized as the primary route of aqueous humor outflow in most primates, including humans. The conventional outflow pathway accounts for approximately 80-90% of total aqueous humor drainage in the human eye, making it the primary determinant of intraocular pressure[9,10].

Intraocular pressure

Intraocular pressure is the fluid pressure within the eye and is maintained as a delicate balance between the production and drainage of aqueous humor[11]. While relatively rare, low intraocular pressure can impair vision by distorting the retina, lens, and cornea. On the other hand, elevated intraocular pressure, which is more prevalent in the general population, can lead to glaucomatous optic neuropathy[7]. Intraocular pressure represents the force exerted by the aqueous humor on the internal surface area of the anterior eye, as pressure is a measurement of force per unit area. This relationship can be theoretically reduced to and explained by the Goldmann equation (IOP = (F/C) +P), where IOP represents intraocular pressure, F represents the rate of aqueous humor formation, C represents aqueous humor outflow, and P denotes the episcleral venous pressure. Any changes or fluctuations in these variables can inevitably impact intraocular pressure[12]. The rate of aqueous humor formation can be influenced by various environmental factors and physiological systems (e.g., ciliary body function, autonomic nervous system, blood flow, etc.)[13]. These systems have been the subject of extensive study and therapeutic targeting for decades and play and important role in the regulation of intraocular pressure[14]. The episcleral venous pressure is another important variable for the determination of intraocular pressure. However, fluctuations in this variable show less correlation with changes in intraocular pressure and are often secondary to an underlying condition. Instead, the homeostatic regulation of intraocular pressure relies primarily on the control of aqueous humor outflow through the conventional outflow pathway and has been the subject of study and therapeutic targeting in more recent years[15]. The conventional outflow pathway is well-established as the primary site of resistance to the outflow of aqueous humor. This resistance is responsible for maintaining intraocular pressure and is essential for overall eye health and function.

The conventional outflow pathway

The conventional outflow pathway, primarily composed of the trabecular meshwork and Schlemm's canal, is the major outlet by which aqueous humor exits the eye. The trabecular meshwork is a filter-like structure located in the anterior chamber of the eye. It is composed of fenestrated beams and sheets made from extracellular matrix that also serve as structural scaffolds on which trabecular meshwork cells reside on. Anatomically, the trabecular meshwork is divided into 3 major anatomical regions known as the uveoscleral meshwork, corneoscleral meshwork, and juxtacanalicular tissue (**Figure 1**). The uveal meshwork consists of a loosely organized network of connective tissue beams that are covered by trabecular meshwork cells. The corneoscleral meshwork is composed of a series of sheets of collagen and elastin which are covered by a monolayer of trabecular meshwork cells. The innermost region of the trabecular meshwork is the juxtacanalicular tissue, directly attached to the inner wall endothelium of Schlemm's canal. In contrast to the cells residing on the uveal and corneoscleral meshwork, juxtacanalicular cells do not form monolayers. Instead, these cells are embedded within an amorphous extracellular matrix and are connected to one another via cellular processes. They also make attachments to the elastin network extending from the anterior tendons of the ciliary muscle[16,17].

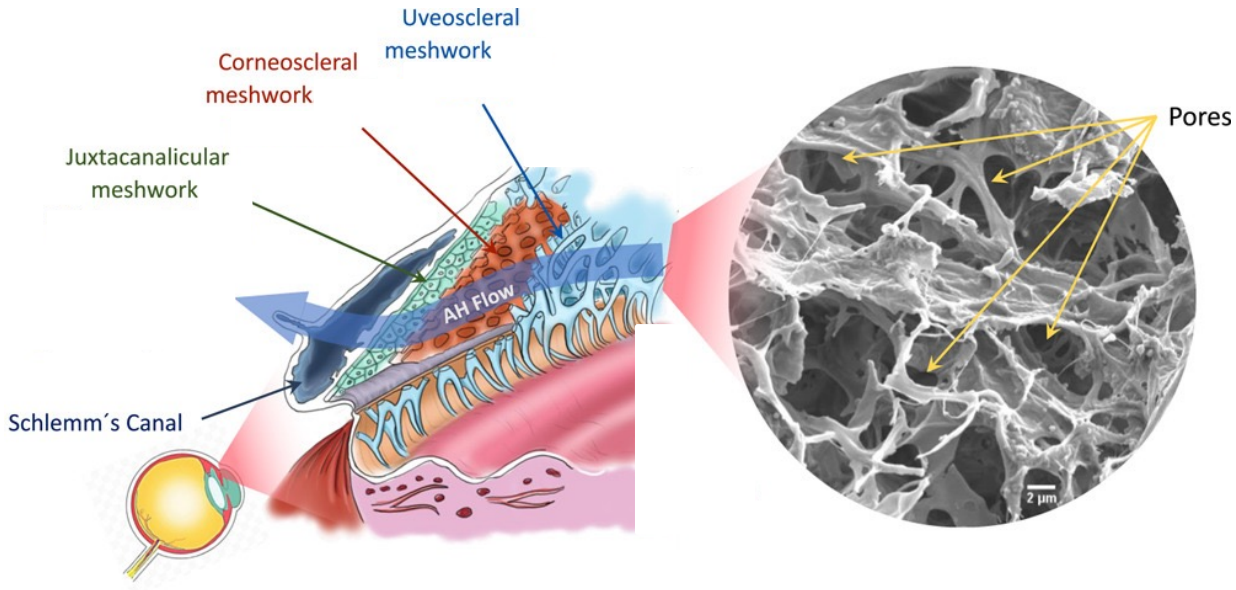

Figure. 1. Anatomy of the trabecular meshwork. The trabecular meshwork is divided into 3 major anatomical regions: the uveoscleral meshwork, corneoscleral meshwork, and juxtacanalicular meshwork. Scanning electron microscopy image shows a real image of decellularized trabecular meshwork tissue and the arrows point to the pores through which aqueous humor flows through. The image was adapted from Bikuna-Izagirre et. al., 2022. Scale bar: 2 µm.

Importance of trabecular meshwork contractility for the regulation of intraocular pressure

Intraocular pressure is a critical parameter for maintaining the health and function of the eye. The delicate balance between the production and drainage of aqueous humor plays a pivotal role in regulating intraocular pressure. Among the key components involved in this process, the contractile properties of the trabecular meshwork play a crucial role in determining outflow resistance and subsequently influencing intraocular pressure. It is generally believed that the contraction of trabecular meshwork cells reduces the size of the intercellular spaces through which aqueous humor travels, creating a higher resistance to the outflow of aqueous humor and increasing intraocular pressure. Conversely, the relaxation of trabecular meshwork cells has the opposite effect. These contraction and relaxation cycles are enabled by the trabecular meshwork's well-developed actomyosin system. As a result, any alterations in the contractile properties of the trabecular meshwork can significantly influence outflow resistance and subsequently impact intraocular pressure. Studies have shown that changes in the contractility of trabecular meshwork cells can be associated with variations in intraocular pressure. Understanding the cellular mechanisms of trabecular meshwork contractility is essential for developing targeted therapeutic interventions for conditions associated with abnormal IOP. In summary, the contractile properties of the trabecular meshwork play a pivotal role in the regulation of intraocular pressure. The dynamic interplay of cellular contraction and relaxation within this tissue directly influences outflow resistance, impacting the delicate balance of aqueous humor dynamics. Further exploration of the mechanisms governing trabecular meshwork contractility holds promise for advancing our understanding of IOP regulation and developing targeted interventions for conditions affecting ocular health[18–21].

Steroid Induced Ocular Hypertension

Steroid-induced ocular hypertension refers to an increase in intraocular pressure resulting from the administration of corticosteroid medications. Corticosteroids, powerful anti-inflammatory drugs, are commonly employed to address various medical conditions, including eye-related issues like uveitis or post-operative inflammation. Whether applied topically (e.g., through eye drops) or administered systemically (e.g., orally, or intravenously), these medications can lead to elevated intraocular pressure, a significant concern due to its association with the development of glaucoma. Glaucoma, a group of eye diseases characterized by progressive optic nerve damage, is often linked to heightened intraocular pressure. The optic nerve is crucial for transmitting visual information from the eye to the brain, and its damage can result in vision loss and even blindness. Steroid-induced ocular hypertension is associated with pathological changes in the trabecular meshwork, including fibrosis. Notably, glucocorticoids, a type of corticosteroid, contribute to increased extracellular matrix deposition and stiffness, influencing the contractility of trabecular meshwork cells. Of particular interest is the potential role of agents capable of modulating the actomyosin system to reduce the contractile phenotype of trabecular meshwork cells. This modulation has shown promise in mitigating the pathological effects induced by glucocorticoids, providing a potential avenue for therapeutic intervention. Understanding the cellular mechanisms underlying steroid-induced ocular hypertension is crucial for developing effective strategies to manage and prevent associated risks, especially in terms of glaucoma. Vigilant monitoring of intraocular pressure and exploration of interventions targeting the trabecular meshwork's contractile features hold promise for optimizing the safety and efficacy of corticosteroid treatments for eye conditions.

Chapter 2: Human trabecular meshwork tissue dissection and explant culture

Explant migration stands as the preferred method in the field of trabecular meshwork biology for establishing cells in primary culture. This approach has proven successful across a variety of species including non-primates, monkeys, and humans[22,23,24]. Over the years, significant efforts have been dedicated to optimizing tissue isolation and explant culture conditions. However, a comprehensive understanding of iridocorneal angle's anatomy, the nuances of tissue isolation, and the precise conditions for explant culture remains essential for the successful establishment of these unique cells.

Anatomy of the Angle

A comprehensive understanding of the anatomy of the trabecular meshwork and its neighboring tissues in the iridocorneal angle is vital when isolating this tissue from corneoscleral rims. The trabecular meshwork is situated within the scleral sulcus, positioned between the scleral spur and the Schwalbe's line, enveloping the Schlemm's canal. The posterior-most layer of the trabecular meshwork, referred to as the uveal meshwork, extends from the ciliary body in the angle recess to the Schwalbe's line, connecting with the scleral spur, the anterior surface of the ciliary body, and indirectly with the root of the iris. The corneal endothelium, though indirectly connected to the trabecular meshwork, terminates at the Schwalbe's line. Directly beneath the uveal meshwork is the corneoscleral meshwork, which extends from the scleral spur to the anterior wall of the scleral sulcus[25]. The anterior-most layer of the trabecular meshwork, known as the juxtacanalicular tissue, overlays the inner wall endothelium of the Schlemm's canal[26]. The small and delicate nature of the trabecular meshwork, coupled with the intricate interconnectedness of the tissues at the iridocorneal angle, presents a unique challenge during tissue extraction, as inadvertently

including neighboring tissue contaminants must be avoided. Therefore, a meticulous examination of the isolated tissue is imperative to minimize the inclusion of such contaminants.

Tissue Isolation

The trabecular meshwork is commonly isolated from corneoscleral rims discarded from corneal transplants, although whole globes or isolated anterior segments can also serve as sources. This tissue usually appears translucent but varies in pigmentation, ranging from light to dark brown. It's important to note that this pigmentation pattern does not apply to individuals with blue eyes. Separating it from corneoscleral tissues is achieved through sharp dissection using scalpels or specialized tools like the kahook-dual blade, or blunt dissection employing dull and sharp-point forceps. Often, a combination of tools in used to ensure a clean and effective separation from surrounding tissues[17]. Luckily, most tissue contaminants that may be included during the isolation of the trabecular meshwork can be spotted and removed with relative ease. The corneal endothelium has a reflective and crystalline appearance, and it can be scraped away from the Schwalbe's line with a scalpel or sharp-point forceps. If present in culture, the hexagonal shaped cells from this tissue typically die after a few days in culture. The sclera has a characteristic milky white appearance and can be avoided by not pushing the forceps too deep into the corneoscleral rim. However, if encountered, it can also be removed from the trabecular meshwork using forceps. The iris can be easily spotted by its brownish, fuzzy-like appearance and grasped at its root before being effectively severed from the ciliary body using a scalpel or scissors. One notable exception to the identification and removal of tissue contaminants is the Schlemm's canal inner wall endothelium, which attaches directly to the juxtacanalicular region of the trabecular meshwork. Interestingly, seminal studies found that while the endothelial lining of the Schlemm's canal remains relatively unchanged during the first days after explantation, it degenerates and disappears after 5-7 days in culture. This makes the endothelial cells of the inner wall of the Schlemm's canal less likely to be present in explant cultures. Intriguingly, this disappearance and

degeneration behavior could also be observed for the uveal and corneoscleral meshwork but not the juxtacanalicular tissue of the trabecular meshwork[27].

Explant Culture

Over the years, extensive work has gone into optimizing the establishment of trabecular meshwork cells from explant cultures. Several approaches have been employed to improve this technique. These include coating the tissue culture dishes with collagen or gelatin to facilitate tissue adhesion and cell migration, using a sterile glass coverslip to weigh down the tissue, or placing tissue strips on the bottom of a dry well for a few minutes to allow for adhesion before carefully adding media[17,28].

A modified approach has been employed in our laboratory which involves the initial delivery of 150 µL of media onto gelatin coated wells in a 24-well plate, followed by the placement of the tissues into the central wells, intentionally avoiding the outer edge wells, which are then filled to near capacity with sterile water to maintain high humidity. This modified approach eliminates the need for a glass coverslip, prevents tissue floating, and minimizes the risk of the tissue drying out. While the usage of bacterial collagenase and/or dispase to encourage cell migration from the explants is employed in the field, our laboratory has omitted this step, as similar results were obtained without enzyme treatment. It's important to note that when enzyme treatment is considered, the use of high-quality collagenase with minimal tryptic and caseinase activity is crucial. The standard explant culture media consists of low glucose DMEM (1g/L), 2mM L-glutamine, and 20% FBS with antibiotic and antimycotic agents. Although some labs supplement with fibroblast growth factors such as bFGF/FGF-2, we have achieved success using 20% FBS alone, without the need of additional growth factors[17].

After the initial isolation and culturing of the tissues, the migration and growth of the trabecular meshwork cells from these explant cultures are systematically monitored through periodic

examinations. This monitoring is carried out with the aim of minimizing any disturbances that might lead to the detachment of the explants from the culture wells. Bright-field or phase-contract microscopy is utilized for monitoring the cultures. Approximately 2 weeks are required for the first signs of cell migration to become evident. It's important to note that the trabecular meshwork, particularly in adult humans, may be accompanied with a variety of cell types beyond trabecular meshwork cells. These may include Schlemm's canal endothelial cells, ciliary muscle cells, corneal endothelial and fibroblast cells, scleral fibroblasts, scleral spur myofibroblasts, scleral vascular or collector channels cells, and macrophages[17,23,24]. Therefore, there exists a genuine possibility that in a culture setting, a slow proliferating population of trabecular meshwork cells could be outcompeted by faster-growing contaminants. To mitigate the risk of contaminant cells from outcompeting trabecular meshwork cells, the tissues are removed once the explant cultures are surrounded by cells, and the culture media are replaced every 2-3 days. Following the initial observation of cell migration at the 2-week mark, an additional 2-3 weeks are required for the cells to reach 80-90% confluence in the wells.

In total, the behavior of over 500 trabecular meshwork tissue explants were examined, sourced from 127 donor eyes. Among these tissue samples, approximately 70% exhibited satisfactory cell migration from the explant cultures and successfully established cell colonies within the cell culture wells. However, approximately 30% of the samples showed no signs of cell migration or proliferation within a two-week period. Any tissues that did not exhibit these crucial signs of growth were promptly discarded to maintain the integrity of our study.

Materials and Methods

The procurement and use of human eye tissues were approved by the University of California Institutional Review Board, and all the experiments were performed in accordance with the tenets of the Declaration of Helsinki for the use of human tissues. The corneoscleral rims used for this study were sourced from various eye banks in collaboration with the Jules Stein Eye Institute at the University of California, Los Angeles. All corneoscleral rims were obtained from healthy donors, kept at 4°C in Optisol-GS storage media (Chiron Ophthalmics Inc., Irvine, CA), and dissected within 3 days of tissue receipt in accordance to the consensus[28,17]. Taking sterile precautions, corneoscleral rims were submerged in low glucose DMEM (1g/L-D glucose; GlutaMAX™ Supplement; 110 mg/L Sodium Pyruvate; Gibco; Thermo Fisher Scientific) on a sterile charcoal dissection dish under a Leica S6E stereomicroscope (**Fig. 2A**). If present on the corneoscleral rims, corneas were punched out using a trephine. The corneoscleral rims were then cut into 4 wedges of similar size using fine-tip scissors, corresponding to the superior, inferior, nasal, and temporal areas (**Fig. 2B**). The corneal endothelia were scraped away from the Schwalbe's line toward the center of the peripheral cornea, and the iris roots were severed from their attachment to the ciliary body to remove potential tissue contaminants (**Fig. 2C**). The trabecular meshwork tissues were grabbed from the edges of the cut wedges by placing one tip of a straight 1.5 mm dull finish platform tying forceps into the Schlemm's canal lumen and the other tip on the posterior trabecular meshwork. The trabecular meshwork tissues were gently pulled away, effectively separating them from the scleral spur and Schwalbe's line, and thereby exposing the Schlemm's canal (**Fig. 2D**) to generate continuous explants of trabecular meshwork approximately 1 cm in length (**Fig. 2E**). The process was then repeated until the trabecular meshwork had been entirely removed from all the wedges (**Fig. 2F**). The tissues were washed in several changes of low glucose DMEM for the removal of any extraneous debris or tissue fragments. The tissues were placed in the center wells of a 24-well plate (Corning; Thermo Fisher

Scientific), which had been previously coated with 0.5% gelatin (Type B; 2% gelatin in H_2O; Sigma-Aldrich), diluted in molecular biology grade water (Water; Low Endotoxin; VWR), for 30 min and allowed to dry for 1-2 hours. The wells were then filled with 150 µL of low glucose DMEM containing 20% FBS (Premium Grade FBS; VWR) and 1X antibiotic-antimycotic (Antibiotic-Antimycotic 100X; Gibco; Thermo Fisher Scientific). Molecular biology grade water was used to fill all remaining wells in the plate to maintain high humidity and prevent the explants from drying. The explant cultures were kept at 37°C in a humidified atmosphere with 5% CO_2. After a week of minimal disturbance to allow the explants to adhere to the surface of the wells, the media were changed every 2-3 days.

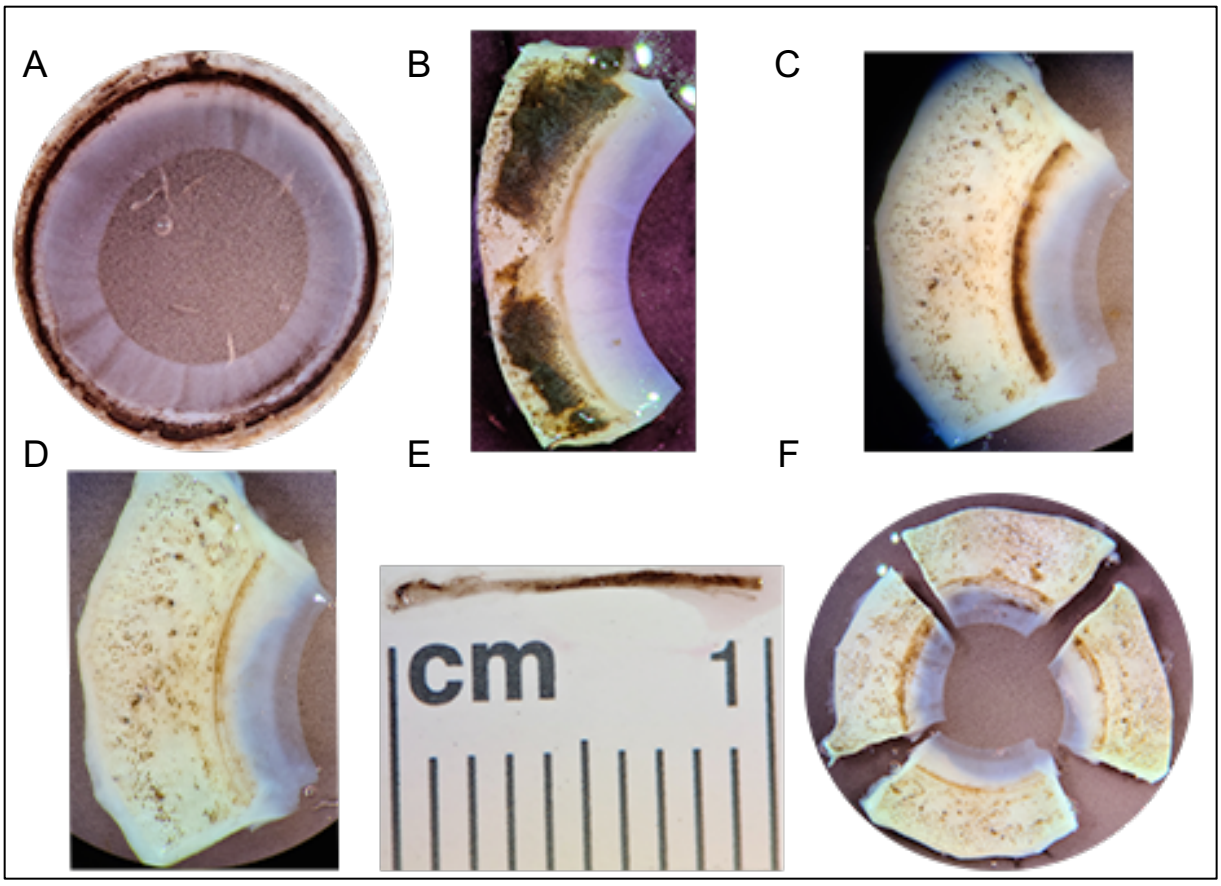

Fig. 2. Removal of the trabecular meshwork from a corneoscleral rim for explant culture. **(A)** Corneoscleral rim on a sterile charcoal dissection dish shown under a Leica S6E stereomicroscope. **(B)** Corneoscleral wedge prior to clean-up and removal of trabecular meshwork. **(C)** Corneoscleral wedge post clean-up, with trabecular meshwork shown as translucent brown pigmented strip. **(D)** Corneoscleral wedge after trabecular meshwork tissue removal. **(E)** Isolated trabecular meshwork tissue strip shown on a ruler, approximately 1 cm in length. **(F)** Cut corneoscleral rims after trabecular meshwork removal from all wedges.

Chapter 3: Establishment of human trabecular meshwork cells in primary culture

Cultured trabecular meshwork cells serve as a valuable model system for investigating the cellular mechanisms that govern the regulation of the conventional outflow pathway, and consequently, intraocular pressure. Culturing these cells facilitates the exploration of their morphology, gene and protein expression, behavior, and responses to diverse stimuli. Nevertheless, the culture and expansion of trabecular meshwork cells requires a keen awareness of the unique challenges and considerations inherent to working with these specialized cells.

Morphology

The morphological characteristics of human trabecular meshwork cells in primary culture have remained a subject of ongoing debate for decades, weaving a complex narrative of research findings and interpretations. Seminal studies conducted by various research groups employing a wide spectrum of imaging techniques revealed intriguing variations in the morphology of these cells. In some investigations, these cells consistently exhibited a broad, flattened, and elongated appearance, often featuring multiple cell processes that occasionally overlapped. This singular, predominant morphology became a hallmark of many subsequent morphological studies. Remarkably, it was also noted that the characteristics of trabecular meshwork cells in vitro closely paralleled those observed in-situ. These resemblances encompassed similar cell surface features, cell junctions, cytoplasmic organelle composition, and nuclear chromatin patterns. Even more strikingly, many of these cellular features persisted even after multiple passages in culture. Notably, during the active division or early confluency stages, trabecular meshwork cells exhibited a heterogenous appearance, posing challenges in distinguishing them from other cultured cell types. The full appreciation of trabecular meshwork cell morphology became evident 7 to 10 days

after cultures reached confluence. At this point, these cells assumed a relatively stable elongated morphological appearance that could be maintained for over a month in vitro. One notable distinction was that trabecular meshwork cells in vitro appeared more densely packed compared to their in-situ counterparts. It was postulated that this difference might arise from the fact that in-situ, trabecular meshwork cells surround a 3-dimensional collagenous core, whereas in a cell culture dish, these cells divide on a single 2-dimensional plane until constrained by neighboring cells. Despite differences in packing density, many distinctive morphological features were maintained in cell culture conditions. As a result, it was firmly concluded that utilizing these cells in vitro offered valuable insights into the structural and functional properties of trabecular meshwork cells in their native environment[22,29,30,31,32].

In contrast, other research groups reported a remarkable diversity within the in vitro cell population, identifying at least 5 morphologically distinct cell forms. These forms included cells with pronounced pseudopodia, ovoid-shaped cells, spindle-shaped cells, cells adorned with distinctive ruffles, and round cells characterized by multiple processes. The mobile, fast-moving cells with pseudopodia were identified as connective tissue macrophages. The ovoid-shaped cells, exhibiting an epithelioid-like locomotion, resembled corneal endothelial cells. Meanwhile, the round multi-process cell form, the spindle-shaped form, and the cells with distinctive ruffles were deemed to be trabecular meshwork cells. Other reported morphologically distinct cell forms included epithelioid-shaped and spherical-shaped cells[33,34]. Further ultrastructural studies unveiled distinct features in cultured human trabecular meshwork cells, notably characterized by nuclei with little heterochromatin content, cytoplasm rich in lysosomal inclusions, numerous small mitochondria, a well-developed Golgi apparatus, abundant polyribosomes, distinctive rough endoplasmic reticulum, and microtubules, a feature rarely observed in their in-situ counterparts. These cellular characteristics appeared to deviate from the typical attributes of trabecular meshwork cells in their native physiological environment, bearing a closer resemblance to

'activated' trabecular meshwork cells often associated with various pathological conditions and injuries. Based on these morphological differences, questions naturally arose about the validity of extrapolating information learned from primary culture trabecular meshwork cells to their in vivo counterparts. Intriguingly, it was noted that after repeated subculture, confluent cultures could be produced in which the cells were morphologically similar to normal human trabecular meshwork cells[23,24,35,36].

During the time these studies were conducted, consensus was lacking regarding the culture conditions for these cells. As a result, variations in basal media, the inclusion of growth factors, animal extracts, and serum, among other factors, may have contributed to observed differences. Today, a consensus has emerged regarding the morphology of trabecular meshwork cells in primary culture. When cultured under current standard conditions, which comprise low-glucose DMEM (1g/L), 2mM L-glutamine, and antibiotic and antimycotic agents, supplemented with 10% fetal bovine serum, these cells typically exhibit cobblestone-like, elongated, or a combination of cobblestone and elongated morphologies, reminiscent of their in-situ counterparts. These morphological characteristics are more evident in earlier passages. Therefore, it is not recommended to culture these cells past passage 7, as they begin to show signs of senescence, such as the presence of vacuoles and an increase in cell size. It's worth emphasizing that, even under standardized culture conditions, trabecular meshwork cells continue to display a variety of morphologies, underscoring the intricate and multifaceted nature of these cells[17,37,38].

Cell Markers

While morphological studies have provided valuable insights into identifying trabecular meshwork cells, relying solely on morphological analysis is insufficient due to the absence of distinctive features. Consequently, the quest for marker proteins specifically identifying trabecular meshwork cells has been a focal point of research since the establishment of human trabecular meshwork

cells in primary culture. Despite decades of dedicated research, the discovery of a single, definitive marker remains elusive. Consequently, researchers have come to depend on a combination of positive and negative selection markers that characterize trabecular meshwork cells both in-situ and in vitro.

Several proteins have been identified as preferentially expressed by trabecular meshwork cells, including Aquaporin-1, α-2A-adrenergic receptor, Collagen IV, Alpha-B crystallin, and Myocilin[37]. These proteins exhibit differential expression or induction in trabecular meshwork cells compared to neighboring cell types, such as ciliary muscle cells, scleral spur cells, scleral fibroblasts, Schlemm's canal endothelial cells, and corneal endothelial cells. Other previously reported trabecular meshwork cell protein markers include Matrix GLA protein, Chitinase-3 Like-1, α-Smooth muscle actin, Smooth-muscle myosin II, and Angiopoietin-like 7[39,40,41,42,43].

Additionally, there are a few marker proteins that trabecular meshwork cells do not express, which are used as negative selection markers. For example, endothelial proteins like PECAM-1, VE-cadherin, Integrin α6, VEGFR3, Prox-1, and Fibulin-2 are expressed by Schlemm's canal cells but not by trabecular meshwork cells. Similarly, epithelial proteins like Keratin and Desmin are not expressed by trabecular meshwork cells[37].

Recent advances in single-cell RNA sequencing technologies have led to the most recent scientific reports attempting to identify specific markers for trabecular meshwork cells. These markers include Phosphatase 1 Regulatory Subunit 1B, Transmembrane Protein with EGF Like and Two Follistatin Like Domains 2, Podoplanin, Retinoic Acid Receptor Responder 1, Fatty Acid-Binding Protein 4, and R-spondin-2. Unfortunately, these proteins are not uniformly expressed by all trabecular meshwork cells but rather by specific subpopulations. Furthermore, their expression has primarily been confirmed in frozen tissue sections, lacking comprehensive characterization across various trabecular meshwork cell strains and passages, as well as in response to diverse stimuli. In some cases, interesting genes were detected in single-cell RNA sequencing studies,

but their presence was confirmed only at the transcript level via in-situ hybridization and their corresponding proteins were not detected[44,45].

Trabecular meshwork cells display expression patterns characteristic of endothelial cells, fibroblasts, smooth muscle cells, and macrophages. It is hypothesized that this multifaceted expression profile stems from their involvement in various functions and their presence in two distinct anatomical environments dedicated to maintaining intraocular pressure homeostasis. The complexity of their expression profile has posed a significant challenge in the quest for a definitive marker, despite years of research. Nonetheless, the similarity in transcriptomic and proteomic profiles between these cultured cells and their in-situ counterparts, even in the absence of a definitive marker, underscores the continued relevance of trabecular meshwork cells in primary culture[46].

Response to various stimuli

In addition to marker proteins, specific responses and behaviors to diverse stimuli help further define trabecular meshwork cells. For instance, TGFβ treatment increases the expression of Plasminogen activator inhibitor-1, Matrix Metalloproteinase 2 protein, and Myocilin in these cells. Moreover, trabecular meshwork cells consistently upregulate Matrix Metalloproteinase 3 & 9 when exposed to IL-1α, TNFα, or the phorbol ester PMA[37]. Another distinctive feature of trabecular meshwork cells, not shared with other ocular cells like corneal endothelial and stromal cells or scleral cells but shared with macrophages, is their uptake of in vitro modified LDL, such as acetylated LDL or acetoacetylated LDL. This behavior has been observed both in vitro and in vivo. The receptors for modified LDL, known as scavenger receptors, are distinct from native LDL binding sites. Similar to macrophages, trabecular meshwork cells are avid phagocytes capable of engulfing a wide variety of materials. It has been postulated that this behavior may be crucial for clearing extracellular debris and remodeling the extracellular matrix under physiological and

pathological conditions. Additionally, like macrophages, trabecular meshwork cells constitutively express MHC class I but not class II complex antigens. However, the expression of class II antigens can be induced by incubation with IFN-γ[47]. Lastly, another remarkable characteristic of trabecular meshwork cells is their ability to neutralize reactive oxygen species. This ability is highlighted by the expression of a number of oxidative-reducing agents, such as superoxide dismutase, glutathione reductase, and peroxidase[37].

Among the various markers considered for identifying trabecular meshwork cells, the most distinctive and universally accepted is the expression of myocilin and its robust upregulation in response to glucocorticoid treatment. Originally referred to as the *TIGR* (trabecular meshwork-induced glucocorticoid response) gene[48,49], myocilin is a protein renowned for its significantly higher expression in trabecular meshwork cells compared to neighboring cells. While the expression of myocilin gradually diminishes over time in cell culture conditions, what makes it particularly intriguing is that trabecular meshwork cells upregulate its expression to exorbitant levels when exposed to glucocorticoids, even if its expression has been lost in culture. This remarkable feature is not shared by neighboring cells. Consequently, the induction of myocilin by glucocorticoids is considered the gold standard and the most reliable method used today for identifying trabecular meshwork cells. This induction typically involves the addition of the glucocorticoid dexamethasone to the culture media at concentrations ranging from 0.1-0.5 μM, mimicking the anticipated aqueous humor concentration subsequent to the application of topical 0.1% dexamethasone phosphate eye drops[50]. Fresh additions are administered every 2-3 days for up to 7 days. This regimen consistently triggers a time-dependent and robust myocilin induction, which can be tested via Western immunoblotting, PCR, or ICC.

Our approach for culturing and characterizing trabecular meshwork cells in primary culture has primarily been focused on evaluating morphology, and the induction of myocilin, although we recognize the significance of the broader criteria discussed above. By prioritizing these critical

attributes, our intent has been to obtain authentic insights into the behavior and characteristics of these cells in vitro that could be relevant in vivo while acknowledging the multifaceted nature of trabecular meshwork cells and the complexities associated with culture conditions.

Materials and Methods

After the initial observation of cell migration at the two-week mark and the establishment of cell colonies in the culture wells, the tissue explants were extracted. An additional period of 2 to 3 weeks was necessary for the cells to attain 80-90% confluence within the wells. At this stage, the cells underwent washing with DPBS and trypsinization with 0.25% Trypsin-EDTA (Gibco), followed by splitting at a 1:4 ratio onto 0.5% gelatin coated cell culture vessels for subsequent expansion and characterization. From this point forward, the cells were maintained in cell culture media containing low-glucose DMEM (1g/L-D glucose; GlutaMAX^{TM} Supplement; 110 mg/L Sodium Pyruvate; Gibco; Thermo Fisher Scientific), and 1X antibiotic-antimycotic (Antibiotic-Antimycotic 100X; Gibco; Thermo Fisher Scientific), supplemented with 10% fetal bovine serum (Premium Grade FBS; VWR) (**Fig. 3**). The validation of trabecular meshwork cell cultures was primarily achieved by assessing myocilin induction using 0.1 μM dexamethasone (Dexamethasone; SIGMA) via qRT-PCR and ICC (**Fig. 4 & 5**). Evaluation of positive markers, such as Myocilin, Alpha-B-crystalline, α-Smooth muscle actin, Chitinase-3-Like-1, and Angiopoietin-Like 7, as well as the examination of negative markers including PECAM-1 and VE-cadherin, was conducted via ICC, provided sufficient material was available. Brightfield and epifluorescence images were captured using an ECHO Revolve, or Keyence BZ-X710 microscope.

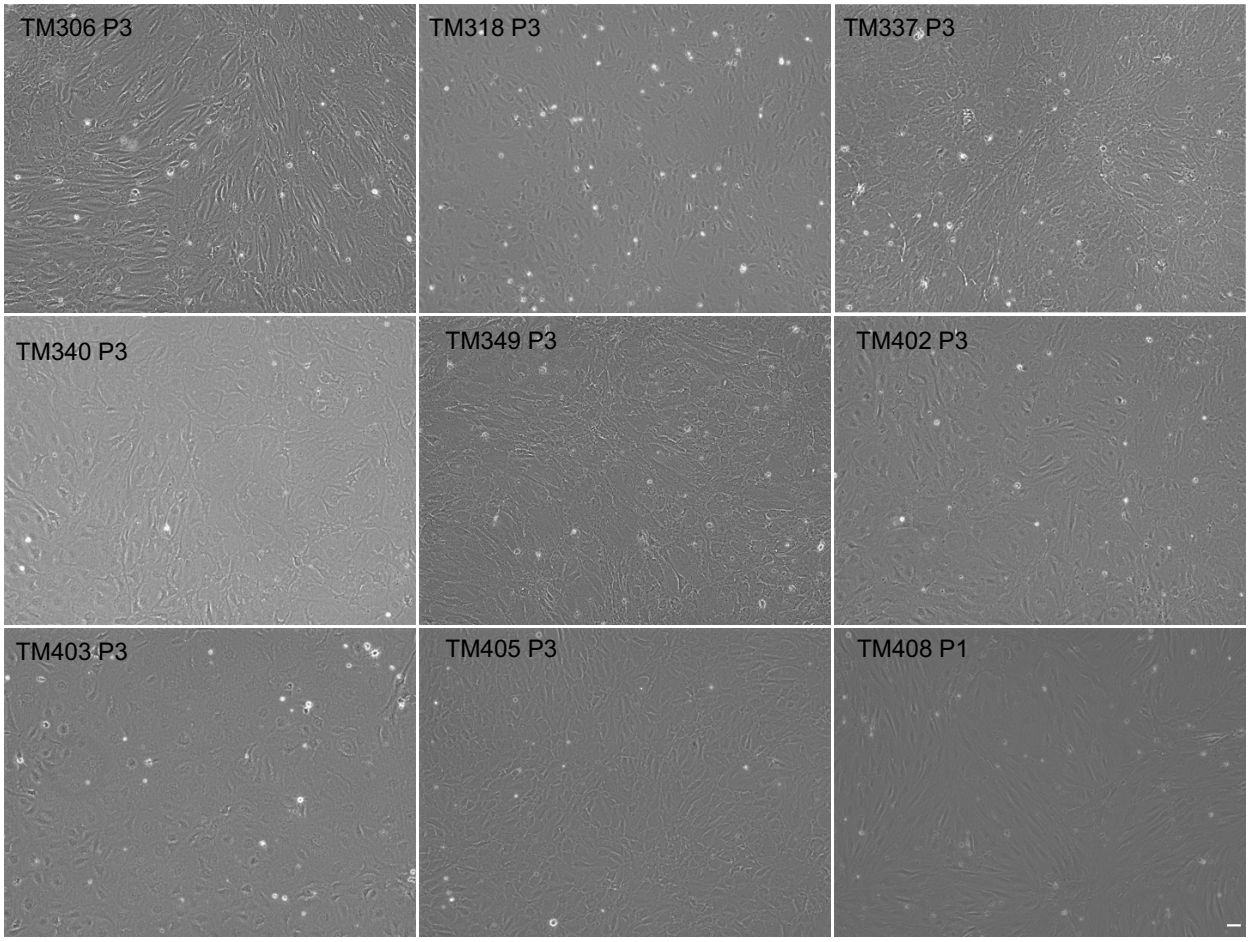

Fig. 3. Representative images of the morphology of human trabecular meshwork cells used for the experiments presented in this thesis. Representative brightfield microscopy images depicting the morphology of human trabecular meshwork cells in culture at passage 1-3. The cells display a mixture of cobblestone, elongated, and fibroblast-like morphologies, often overlapping with one another. All images were captured using a Keyence BZ-X710 microscope at 10X magnification. The scale bar represents 50 μm.

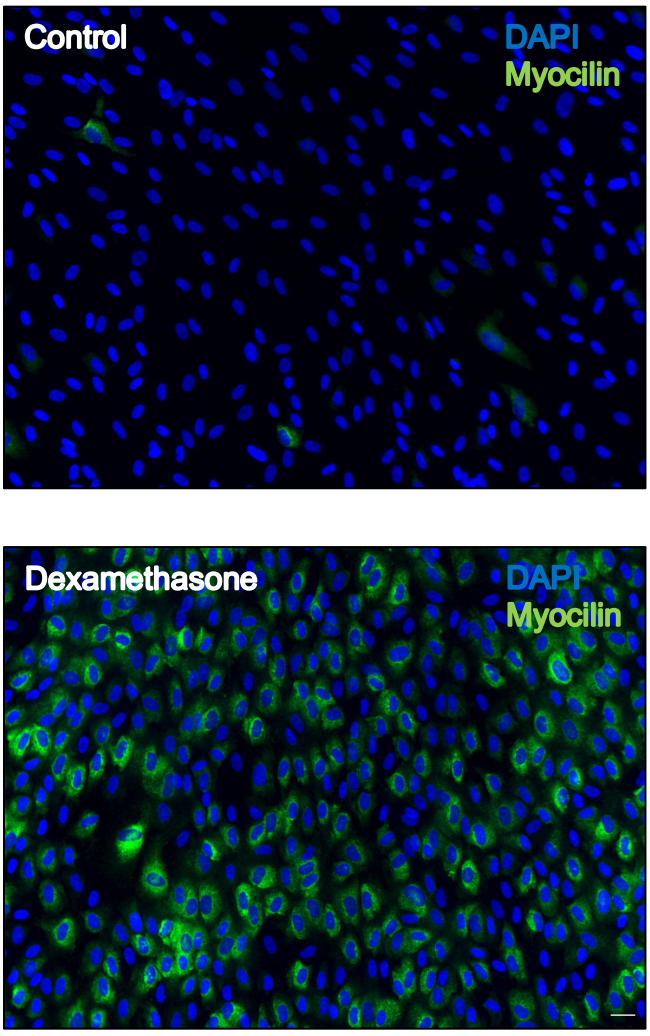

Figure. 4. Representative immunofluorescence images of human trabecular meshwork cells stained for myocilin. Trabecular meshwork cells at passage 3 were treated with either control (0.05% DMSO, top image) or 0.1 μM dexamethasone (bottom image) for 5-days. Following treatment, the cells were fixed, permeabilized, and immunostained using an anti-human myocilin antibody produced in rabbit. An anti-rabbit alexa-488 secondary antibody was used for signal detection and the cell nuclei were counterstained with Hoechst 33342. Dexamethasone treatment robustly upregulated the expression of myocilin in the cells relative to the control. This substantial increase in myocilin expression serves as confirmation of the cells' identity as trabecular meshwork cells. Images were captured using a Keyence BZ-X710 microscope at 10X magnification. The scale bar represents 50 μm.

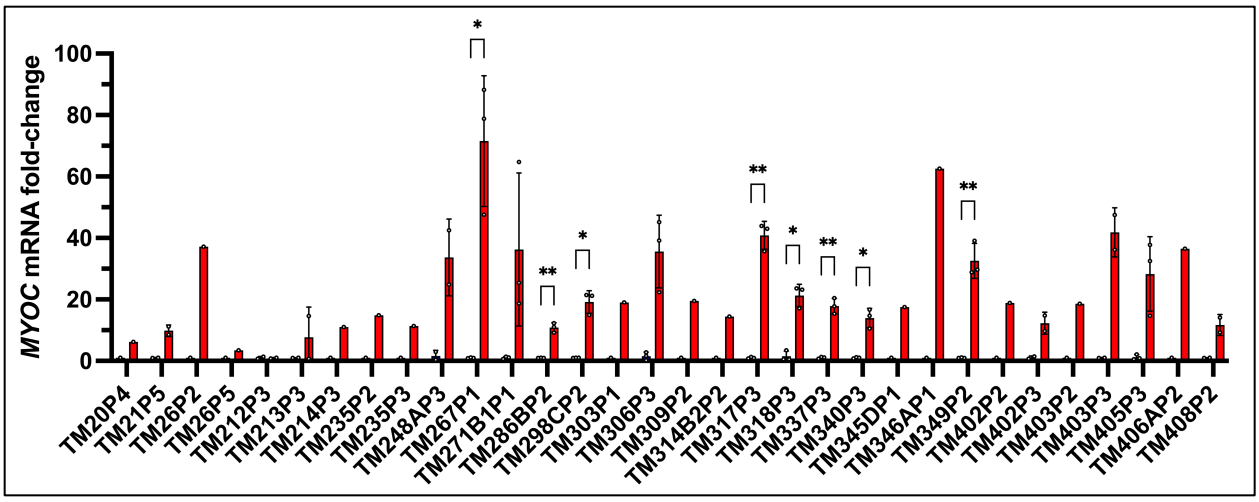

Figure. 5. Assessment of myocilin (*MYOC)* mRNA induction in human trabecular meshwork cells in primary culture after dexamethasone treatment via qRT-PCR. Human trabecular meshwork cells (passage 1-4) were treated with control (0.05% DMSO), or 0.1 μM dexamethasone for 5-days. Experiments were performed in triplicates provided sufficient material was available. After the 5-day treatment, the cells were harvested, and the total RNA was isolated using Qiagen's RNA extraction kit. TaqMan qRT-PCR was performed, and the data was analyzed using the ΔΔ-Ct method. An unpaired t-test of unequal variance was performed to determine significance (*$p<0.05$, **$p<0.005$). The robust upregulation in *MYOC* mRNA indicated that the cells isolated and expanded are in fact human trabecular meshwork cells.

Chapter 4: Optimization of FLECS assay for human trabecular meshwork cells

The effective adaptation and optimization of an assay are pivotal for ensuring the accuracy, relevance, and reliability of experimental findings, contributing to our understanding of cellular processes in normal and disease states, as well as facilitating drug evaluation. This chapter focuses on the critical elements examined for the adaptation and optimization of the FLECS assay for trabecular meshwork cells. Moreover, the chapter delves into the intricacies of data acquisition and analysis, highlighting their significance in ensuring precise and insightful data interpretation. The primary aim of this chapter is to provide insights into the initial strategies and findings that were instrumental in establishing the current workflow, successful execution of the assay, and data analysis.

Workflow for FLECS assay in 24-well plate format

The early version of the FLECS assay was accessible to researchers in 6-well and 24-well plate formats, requiring only a fluorescence microscope capable of capturing high-quality TIFF images, and no other specialized equipment. The workflow primarily involved two major steps: cell seeding and imaging, each demanding adaptation and optimization for specific cell types. The experimental workflow for preparing the FLECS plate began with its acquisition and unpacking inside a biosafety cabinet. Subsequently, the phosphate-buffered saline (PBS) storage buffer was carefully aspirated from the wells, ensuring not to touch the bottom to prevent disruption of the fluorescent micropattern matrix at the well's base. After the removal of the PBS, the wells underwent several washes with cell seeding media to eliminate any potential debris present from the plate fabrication process and to prime the well environment for cell introduction. Next, the wells were filled with media and placed inside an incubator at 37°C. Following the incubation

period, excess media was aspirated, leaving some in the well to about 5 mm above the matrix to prevent it from drying. The cells were then evenly dispensed as individual droplets of cell solution directly onto the well's fluorescent micropattern matrix. A light microscope was employed to assess the cell density and distribution immediately after dispending. The plate was then incubated at 37°C for approximately 1-1.5 hours with minimal disturbance to facilitate cell adhesion to the matrix. Once visual confirmation of cell adhesion was obtained, unadhered cells were washed off from the wells. This was accomplished by tilting the FLECS plate using its lid, and simultaneously dispensing fresh media on one end, while aspirating from the other end. This convective flow induced mild sheer stress over the cells, dislodging weakly adhered cells not attached to the fluorescent micropattern matrix. The cells were then immersed in media and placed back in the incubator until they were ready for imaging. Before image acquisition, a cell permeable nuclear stain, Hoechst 33342, was introduced into the media. Finally, using a fluorescence microscope, overlayed images of the fluorescent micropatterns and the cell nuclei were captured from every well and saved as TIFF files.

The preliminary assessment of the assay workflow identified specific steps that would require optimization for the adaptation of this assay for trabecular meshwork cells. These included determining the appropriate substrate material, size, and stiffness for the fabrication of the fluorescent micropatterns, selecting a suitable cell culture media, defining the ideal cell density, and adjusting the stringency of the washes, and fine-tuning the incubation times. Additionally, careful considerations for image magnification, acquisition process, and subsequent analysis would need to be considered.

70 µm ‘X’-shaped Fibronectin Micropatterns Pilot Experiment

The FLECS assay’s ‘X’-shaped fluorescent micropatterns were initially fabricated using an equal parts mixture of fibronectin and Alexa-Fluor 568 labeled fibrinogen. These micropatterns featured a diagonal dimension of 70 µm and a thickness of 10 µm[51]. The robustness and repeatability of the micropatterns’ fabrication using this formulation was undeniably successful with defects occurring in less than 1% of the patterns. Fibronectin is a versatile ECM protein that plays a critical role in various cellular processes, including cell adhesion, migration, proliferation, differentiation, and tissue development and repair. Additionally, fibronectin has long been recognized as the product of cultured trabecular meshwork cells, and a component of the trabecular meshwork tissue’s ECM. Therefore, utilizing fluorescent micropatterns fabricated from fibronectin seemed like a reliable starting point for the adaptation and optimization of this assay for trabecular meshwork cells.

Materials and Methods

Taking sterile precautions, a 24-well FLECS plate (Cat# FZAX1R02Z), containing approximately 24,000 fibronectin ‘X’-shaped fluorescent micropatterns per well, was opened inside a biosafety cabinet. The PBS storage buffer was carefully aspirated from the wells, ensuring that the fluorescent micropattern matrix at the well’s base was not disturbed. The wells were washed 3-times with 20% FBS TM media to eliminate any potential debris present from the plate fabrication process and to prepare the well environment for cell introduction. Subsequently, each well was supplemented with 1 ml of 20% FBS TM media and placed in an incubator at 37°C under a 5% CO_2 atmosphere. Trabecular meshwork cells isolated from 2 different donors were pre-treated with 0.1% (v/v) DMSO, 0.1 µM dexamethasone, or a combination of 0.1 µM dexamethasone plus 3 µM Wnt inhibitor compound 0367 for 5-days in 20% FBS TM media. After the pretreatment, the cells were washed 3 times with PBS, trypsinized for 5 minutes at 37°C, resuspended in 20% FBS

TM media, counted, seeded at a density of 28,800 cells per well in a 1mL volume. The seeded cells were left to incubate for 1 hour at room temperature, followed by an additional 30-minute incubation at 37°C under a 5% CO_2 atmosphere. Following these incubations, the wells were washed 3 times with 20% FBS TM media to remove unadhered or clumped cells. Subsequently, media containing 0.1% (v/v) DMSO, 0.1 μM dexamethasone, or 0.1 μM dexamethasone plus 3 μM Wnt inhibitor compound 0367 was added back into the wells. The plate was then incubated for 12 hours at 37°C under a 5% CO_2 atmosphere prior to image capture. Hoechst 33342 was added to the wells at a target concentration of 1μg/mL prior to image acquisition. Fluorescence images at 10X magnification were taken using a Keyence BZ-X710 microscope. Images were submitted for analysis to Forcyte Bio.

Results

Trabecular meshwork cells clearly adhered and patterned over the 70 μm 'X'-shaped fibronectin micropatterns, evidenced by the presence of the Hoechst 33342 stained nuclei over the Alexa-Fluor 568 labeled patterns. The cells were uniformly distributed across the entire wells, evidence by the absence of noticeable regions without any nuclei. The trabecular meshwork cells' nuclei were predominantly positioned right at the center rather than the arms or extremities of the micropatterns. In many instances, the cells appeared to form small clumps or congregations, evidenced by the presence of multiple blue nuclei close to one another on a single micropattern. However, there were instances where single cells adhered to a single pattern although this occupancy wasn't consistent across the entire areas examined. All of these features were present on the cells adhered over the micropatterns, regardless of the treatment. Interestingly, trabecular meshwork cells did not appear to robustly contract in either the dexamethasone, dexamethasone plus Wnt inhibitor, or control group by visual examination. This was evident by the lack of inward displacement of the micropatterns' boundaries, which reflect the cells' applied forces. Upon image submission for analysis, we found that dexamethasone treated cells contracted more than

dexamethasone plus Wnt inhibitor 0367 or control treated cells displaying median population contractions of 2.5 μm, 1.9 μm, or 1.2 μm respectively across both donors.

Discussion

In this pilot experiment, we utilized a 24-well FLECS plate containing fibronectin 'X'-shaped fluorescent micropatterns featuring a diagonal dimension of 70 μm and a thickness of 10 μm. The cells' nuclei perfectly overlayed the 'X'-shaped fluorescent micropatterns and were preferentially positioned at the center rather than the extremities of the micropatterns very evenly spaced across the well. This indicated that the cells successfully adhered to fibronectin and could be confined to the micropatterns rather than spreading randomly over the entire surface of the wells. This also meant that the 70 μm 'X'-shaped micropatterns provided enough surface for the cells to attach and spread; although, this had to be further confirmed by brightfield or phase contrast microscopy to ensure the cells were not spreading across multiple patterns.

While patterns with single nuclei were present in the wells, we very commonly noticed the presence of multiple nuclei close to one another over a single micropattern. Since trabecular meshwork cells are mononucleated, we figured that the presence of multiple nuclei on a single micropattern meant that the cells clumped pre or post seeding, actively divided on the micropatterns, or had compromised plasma membranes causing multiple cells to fuse. Very few clumps were observed during cell counting step; however, the cells stayed in the collection tubes for a long time prior to seeding, and so it is possible for the cells to have settled at the bottom of the tubes and clumped prior to seeding. We also considered the possibility for two cells to have landed on a single micropatterns and occupied the same surface. Trabecular meshwork cells have a doubling time of approximately 48 hours; therefore, the active division of the cells on the micropatterns seemed less likely since the images of the cells on the micropatterns were taken at the 12-hour time point but it is possible. The presence of multiple nuclei on a single micropattern could also have been the result of a technical artifact from the sample preparation and the cell

seeding density used. Multinucleated cells in cell suspension can arise from various reasons, and one potential cause is mechanical stress during cell suspension. When cells are subjected to harsh or vigorous resuspension techniques, it might lead to the compromise of the plasma membrane, allowing neighboring cells to fuse and form multinucleated cells. Additionally, the FLECS assay's original protocol suggested a seeding density of 1.2-fold excess of cells to the number of micropatterns; however, this was suggested based on optimization using a different cell type. Therefore, it is possible that this seeding density may not have been optimal for trabecular meshwork cells and needed to be optimized. While trabecular meshwork cells contracted on the fibronectin micropatterns, this contraction was not very robust across all treatments. This result was very intriguing since trabecular meshwork cells share phenotypic similarities with smooth muscle cells and exert strong contractile forces upon stimulation[37,52]. The connective tissue in the trabecular meshwork is composed of several types of ECM proteins such as collagens, glycoproteins, glycosaminoglycans, and elastin. In addition, the Young's modulus of healthy tissue is on the softer side on average 4 kPa but ranges from 0.5-10 kPa. The components and stiffness of the ECM are critical for trabecular meshwork cell function in physiological and pathological states, and changes in these critical factors may affect their behavior. If the matrix is stiff (high Young's Modulus), the cells might generate more contractile forces because they have a rigid structure to pull against. Conversely, if the matrix is more compliant (Low Young's modulus), the cells may not be able to generate as much force because their surroundings are not as supportive. Therefore, it is possible that material and stiffness of the micropatterns may not have been optimal for the cells to exert strong contractile forces. At the time of these experiments, the exact stiffness of the fibronectin micropatterns was unknow to us, but it was most likely below 4-8 kPa within the trabecular meshwork's physiological Young's Modulus.

70 µm ‘X’-shaped Collagen-I Micropatterns Experiment

In our pilot experiment, trabecular meshwork cells adhered, spread, and remained within a 70 µm ‘X’-shaped micropattern. This observation was supported by the perfect alignment of the cells’ nuclei with the micropatterns in an organized manner. This indicated that the micropatterns size provided an adequate surface area for trabecular meshwork cells to attach; however, micropatterns with multiple nuclei were abundantly observed. In addition, fibronectin was an adequate substrate for the cells to attach and contract although this contraction was very subtle. To continue to optimize the seeding density of the cells to obtain the maximal number of single cells over the micropatterns and to continue to explore different materials suitable to the trabecular meshwork cells to attach and contract, we decided to test the use of 70 µm ‘X’-shaped collagen-I micropatterns at 2 different stiffnesses. To do this we employed 2 collagen-I FLECS plates with stiffness levels referred to as R02Z, and R06Z. R02Z was the stiff collagen-I and R06Z was the soft collagen-I FLECS plate.

Materials and Methods:

Taking sterile precautions, 2 different 24-well FLECS plates (Cat#R02Z & Cat#R06Z), containing approximately 24,000 Collagen-I ‘X’-shaped fluorescent micropatterns per well, were opened inside a biosafety cabinet. The PBS storage buffer was carefully aspirated from the wells, ensuring the fluorescent micropattern matrix at the well’s base was undisturbed. The wells were washed 3-times with 10% FBS TM media to eliminate any potential debris present from the plate fabrication process and to prepare the well environment for cell introduction. Subsequently, each well was supplemented with 1 ml of 10% FBS TM media and placed in an incubator at 37°C under a 5% CO_2 atmosphere. Untreated trabecular meshwork cells isolated from a single donor were used for this experiment. The cells were washed 3 times with PBS, trypsinized for 5 minutes at 37°C, resuspended in 10% FBS TM media, passed through a 40 µm cell strainer, counted, and

seeded at a density of 28,800, 24,000, and 19,200 cells per well in a 1mL volume for both plates. The seeded cells were left to incubate for 1 hour at room temperature, followed by an additional 30-minute incubation at 37°C under a 5% CO_2 atmosphere. Following these incubations, the wells were washed 3 times with 10% FBS TM media to remove unadhered or clumped cells. Subsequently, the plates were incubated for 6 hours at 37°C under a 5% CO_2 atmosphere prior to image capture. Hoechst 33342 was added to the wells at a target concentration of 1µg/mL prior to image acquisition. Brightfield and fluorescence images were taken at 10X magnification using a Keyence BZ-X710 microscope.

Results

Trabecular meshwork cells adhered and patterned over the 70 µm 'X'-shaped collagen-I micropatterns on the R02Z and R06Z FLECS plates after the 6-hour incubation time. Overall, a lower number of multinucleated micropatterns were observed across plates and cell seeding densities. An increasing number of cells attached to the micropatterns was observed with increasing cell seeding density. No difference in cell attachment number was observed in the 1.2X and 1X fold cell seeding densities, but a difference was observed with the 0.8X cell seeding density having less cells attached in general. The cells did not display any particular preference in attachment to either the R02Z or R06Z plate. Interestingly, unusual deformities were observed in the R02Z plate which were not present in the R06Z plate. These micropattern deformities hindered our ability to take equal number of images on both plates. Patches of micropatterns without cells were observed across plates and cell seeding densities. However, the patches of micropatterns without cells were less evident with the higher cell seeding density conditions. Interestingly, the cells robustly contracted on collagen-I micropatterns with a tendency to contract more robustly on the R02Z plate over the R06Z plate.

Discussion

In this experiment, we utilized 2 different 24-well collagen-I FLECS plates. These plates featured 'X'-shaped fluorescent micropatterns with a diagonal dimension of 70 μm, an approximate thickness of 10 μm, and stiffness levels referred to as R02Z and R06Z. The exact stiffness of the micropattern matrix was unknow to us but was most likely below 4kPa. The R02Z was the stiff collagen-I, and the R06Z was the soft collagen-I. As previously observed with the 24-well fibronectin FLECS plate, the 70 μm 'X'-shaped micropatterns provided enough surface for the single cells to attach and spread. This was supported by the fact that the cells' nuclei perfectly overlayed the micropatterns in an organized fashion and was further confirmed by brightfield microscopy. No cells were observed attaching across multiple patterns. No difference in cell attachment number was observed in the 1.2X and 1X fold cell seeding densities, but a difference was observed with the 0.8X cell seeding density having less cells attached in general. The reason for trying various seeding densities was to optimize the number of single cells attached to the micropatterns. It seems that a 1:1 cell seeding density ratio or 1.2-fold excess of cells to the number of micropatterns maybe suitable for seeding in the 24-well FLECS plates. Overall, a lower number of multinucleated micropatterns were observed across plates and cell seeding densities. We believe this may be due to a combination of factors changed in our workflow process not having to do with cell seeding densities because less multinucleated cells were observed across all seeding conditions. For instance, the cells were resuspended in 10% FBS media rather than 20% FBS media. High concentrations of FBS can sometimes promote cell aggregation in cell suspensions. This is because FBS contains various proteins and factors that can mediate cell-to-cell interactions. In addition, the cells were thoroughly yet gently resuspended, and passed through a 40 μm cell strainer this time around. Interestingly, unusual deformities were observed in the R02Z plate which were not present in the R06Z plate. These micropattern deformities hindered our ability to take equal number of images on both plates. The deformities observed in

the micropattern matrix may have come from the plate fabrication process or from a disturbance to the matrix at the base of the wells. Patches of micropatterns without cells were observed across both plates and all cell seeding density conditions. This may have been due to the harsher washing conditions performed during the experiment. The cells did not display any particular preference in attachment to neither the R02Z nor R06Z. Although, this is hard to tell since few images were taken on the R02Z plates due to deformities present in wells. Interestingly, the cells appeared to contract on the R02Z plate more robustly, the stiffer collagen-I, rather than the R06Z plate the softer collagen-I plate. We thought that this may be due to the R06Z' soft collagen being too compliant for the cells to be stably supported. The contraction of the cells on the R02Z collagen-I plate was also visually much more robust than on the R02Z fibronectin used in the pilot experiment. Therefore, we believe a collagen substrate may be more for trabecular meshwork cells to attach and contract over the fibronectin. Further experiments needed to be conducted to test the effect of substrate stiffness on cell contraction. However, it seems that a material which is too soft may not be suitable for the cells to exert strong contractile forces.

70 µm ‘X’-shaped Collagen-IV Micropatterns Experiment

Type IV collagen is the main collagen component of basement membranes which play fundamental roles in differentiation, proliferation, survival, and migration of cells during embryonic development, but also serve as selective barriers and structural scaffolds. Collagen type IV forms networks somewhat reminiscent of the hexagonal lattices in chicken wire, which coupled with other basement membrane proteins, is thought to function as a scaffolding for the attachment of cells via specific glycoproteins. In the trabecular meshwork, type IV collagen is found in the basement membranes covering the trabecular beams, underneath the Schlemm’s canal cells along the inner and outer walls, and in the sheath material around the elastin fibers[53]. Collagen IV is also secreted by these cells in culture. Given the importance of this critical ECM protein, and its abundance throughout the trabecular meshwork, we decided to test the ability of the trabecular meshwork cells to attach and contract on 70 µm ‘X’-shaped collagen-IV micropatterns. To do this, we employed 3 collagen IV 24-well FLECS plates each with different stiffness levels categorized as R02Z, R06Z, and R07Z. R02Z was the stiffer collagen IV, followed by R06Z which lied somewhere in the middle, and finally soft R07Z.

Materials and Methods

Taking sterile precautions, a total of 3 Collagen-IV 24-well FLECS plates (Cat#R02Z, R06Z R07Z), containing approximately 24,000 ‘X’-shaped fluorescent micropatterns per well, were opened inside a biosafety cabinet. The PBS storage buffer was carefully aspirated from the wells, ensuring the fluorescent micropattern matrix at the well’s base was undisturbed. The wells were washed 3-times with 10% FBS TM media to eliminate any potential debris present from the plate fabrication process and to prepare the well environment for cell introduction. Subsequently, each well in all 3 plates was supplemented with 1 ml of 10% FBS TM media and placed in an incubator

at 37°C under a 5% CO_2 atmosphere. Untreated trabecular meshwork cells isolated from a single donor were used for this experiment. The cells were washed 3 times with PBS, trypsinized for 5 minutes at 37°C, resuspended in 10% FBS TM media, passed through a 40 µm cell strainer, and counted. The cells were seeded at a density of 36,000, 28,800, or 19,200 cells per well in a 1mL volume, corresponding to a 1.5-fold, 1.2-fold, or 0.8-fold cell excess to total micropatterns, across all 3 plates. The seeded cells were left to incubate for 1 hour at room temperature, followed by an additional 30-minute incubation at 37°C under a 5% CO_2 atmosphere. Following these incubations, the wells were washed 3 times with 10% FBS TM media to remove unadhered or clumped cells. Subsequently, the plates were incubated for 6 hours at 37°C under a 5% CO_2 atmosphere prior to image capture. Hoechst 33342 was added to the wells at a target concentration of 1µg/mL prior to image acquisition. Brightfield and fluorescence images were taken at 10X magnification using a Keyence BZ-X710 microscope. The total number of single nuclei present on the micropatterns from 7 fields of view were calculated across all 3 plates and cell seeding densities. The average number of single nuclei present on the micropatterns per field of view were also calculated along with the standard deviation.

Results

Trabecular meshwork cells adhered and spread over the 70 µm 'X'-shaped collagen-IV micropatterns on the R02Z, R06Z, and R07Z FLECS plates after the 6-hour incubation time. The adherence and spreading were verified by brightfield microscopy. As observed with the collagen I FLECS plates, fewer multinucleated micropatterns were detected across all 3 Collagen IV plates and cell seeding densities. The 28,800 cells/mL seeding density had the largest number of single nuclei per field of view at 10X magnification across all 3 plates averaging 55 +/- 5, 47 +/- 11, and 48 +/- 9 single nuclei per field of view at 10X for the R02Z, R06Z, and R07Z respectively. The 19,200 cells/mL seeding density had the next largest number of single nuclei per field of view at 10X magnification averaging 49 +/- 8, and 46 +/- 15 single nuclei for the R02Z and R06Z plates,

respectively. However, the 19,200 cells/mL seeding density had the fewest number of single nuclei per field of view at 10X in the R07Z plate with a value of 37 +/- 4 nuclei. The 36,000 cells/mL seeding density had the fewest number of single nuclei per field of view at 10X magnification in the R02Z and R06Z plates but was the second largest for the R07Z plate averaging 49 +/- 10, 31 +/- 7, and 41 +/- 17 single nuclei per field of view at 10X. The trabecular meshwork cells preferentially attached to the R02Z plate, followed by the R06Z, and finally the R07Z. Visually, the contraction of the micropatterns was the most robust on the R02Z, followed by the R06Z, and R07Z in this order (**Table 1**).

Discussion

In this experiment, we utilized 3 different Collagen IV FLECS plates. These plates featured 'X'-shaped fluorescent micropatterns with a diagonal dimension of 70 μm, an approximate thickness of 10 μm, and stiffness levels referred to R02Z, R06Z, and R07Z. The exact stiffness of the micropatterns was not provided but it was most likely below 4 kPa for all plates used, within the physiological range. The R02Z plate was the stiff collagen IV, followed by the R06Z which lied somewhere in the middle, and the R07Z was the soft collagen IV. We found that trabecular meshwork cells adhered and spread over the collagen IV fluorescent micropatterns across all 3 stiffness levels tested. Interestingly, the cells preferentially attached to the stiffer R02Z collagen IV FLECS plate, over the other 2 softer collagen IV plates. Visually, the cells exerted stronger contractile forces on the stiff R02Z collagen IV plate. While this result was intriguing, it was not entirely surprising. Trabecular meshwork cells share many phenotypic similarities with smooth muscle cells. Smooth muscle cells preferentially migrate, adhere, and spread toward more rigid substrate regardless of the ECM composition. In addition, upon adherence to a more rigid substrate, smooth muscle cells exert stronger contractile forces. We found this to be true for trabecular meshwork cells in our experiment as well, with the exception that the FLECS assay does not look at cell migration since the cells are confined to the micropatterns.

	Seeding Density		
FLECS R02Z Plate	19,000 cells/mL	28,800 cells/mL	36,000 cells/mL
Field 1	55	59	47
Field 2	45	50	36
Field 3	52	51	57
Field 4	44	56	63
Field 5	56	61	53
Field 6	35	51	37
Field 7	58	60	50
Total	345	388	343
Ave # single cell nuclei per field of view at 10X	49.28571429	55.42857143	49
Stdev	8.280786712	4.720774755	9.949874371
	Seeding Density		
FLECS R06Z Plate	19,000 cells/mL	28,800 cells/mL	36,000 cells/mL
Field 1	59	49	23
Field 2	58	36	28
Field 3	21	36	25
Field 4	33	58	37
Field 5	42	36	32
Field 6	54	57	43
Field 7	56	60	31
Total	323	332	219
Ave # cells per field of view at 10X	46.14285714	47.42857143	31.28571429
Stdev	14.64500565	11.22285084	6.945365018
	Seeding Density		
FLECS R07Z Plate	19,000 cells/mL	28,800 cells/mL	36,000 cells/mL
Field 1	42	44	12
Field 2	32	49	27
Field 3	35	53	36
Field 4	43	45	58
Field 5	38	34	50
Field 6	39	62	52
Field 7	33		56
Total	262	287	291
Ave # cells per field of view at 10X	37.42857143	47.83333333	41.57142857
Stdev	4.276179871	9.410986487	17.20326658

Table. 1. Summary of seeding density optimization results. The 28,800 cells/mL seeding density had the largest number of single nuclei per field of view at 10X magnification across all 3 plates.

Chapter 5: Effects of ECM material on human trabecular meshwork single-cell contractility

In the previous chapter, we provided some insights into the initial strategies and findings that were instrumental for the adaptation and optimization of the FLECS assay for primary human trabecular meshwork cells. We found that trabecular meshwork cells successfully adhered, spread, and remained within 'X'-shaped fluorescent micropatterns featuring a diagonal dimension of 70 μm, and an approximate thickness of 10 μm. A 1:1 seeding ration of cells to micropatterns was determined to be optimal for obtaining the maximal number of single cell attachment. The cells attached to fibronectin, collagen I, and collagen IV micropatterns, consistent with previous studies examining the adhesion of these cells to various extracellular matrix proteins in culture. Trabecular meshwork cells seemed to preferentially attach to stiffer substrates. Intriguingly, compared with cells adhered upon a soft substrate, those adhered upon a stiff substrate exhibited greater contractile forces. We observed this on collagen I and collagen IV FLECS plates, but not on fibronectin since we only tested 1 stiffness for this protein. These results were also based upon the visual examination of the micropatterns since at the time we did not have consistent access to an analysis pipeline to quantitate our images. In addition, the exact stiffness of the micropatterns was unknown but was most likely below 4 kPa. In this section, we aimed to resolve the previous discrepancies we had regarding the appropriate substrate material for trabecular meshwork cells to exert robust contractile forces. Here, we utilized 96-well FLECS plates containing micropatterns fabricated from collagen I, collagen IV, or fibronectin of a stiffness of 4-8 kPa verified by tensile tester across all 3 plates.

Materials and Methods

Taking sterile precautions, a total of 3 96-well FLECS plates fabricated with collagen I, collagen IV, or fibronectin (Cat#96-COL1-AF546-X70-Q1.2, Cat# 96HC4FG546X1Q1.2, Cat# 96-FN-AF546-X70-Q1.2), containing approximately 3,200 'X'-shaped fluorescent micropatterns per well, were opened inside a biosafety cabinet. The PBS storage buffer was carefully aspirated from the wells, ensuring the fluorescent micropattern matrix at the well's base was undisturbed. The wells were washed with 10% FBS TM media to eliminate any potential debris present from the plate fabrication process and to prepare the well environment for cell introduction. Subsequently, each well in all 3 plates was supplemented with 100 µL of 10% FBS TM media and placed in an incubator at 37°C under a 5% CO_2 atmosphere. Untreated trabecular meshwork cells isolated from a single donor were utilized for this experiment. The cells were serum starved for 24 hours prior to the day of the experiment. The cells were washed 3 times with PBS, trypsinized for 5 minutes at 37°C, resuspended in 10% FBS TM media, passed through a 40 µm cell strainer, and counted. A total of 3,200 cells were seeded per well in 100 µL volume of 10% FBS TM media containing 1µg/mL Hoechst 33342. The image acquisition process was performed immediately after a 1-hour incubation at room temperature. Images of the fluorescent patterns and cell nuclei were obtained using an ImageXpress Micro XL High-Content Imaging System fluorescence microscope at 4X magnification. Image analysis was performed on a pipeline available on Biodock AI.

Results

Trabecular meshwork cells rapidly and robustly contracted on the collagen IV micropatterns. The contraction plateaued after 6-hours at which point the cells ceased to contract and stabilized. The contraction values clustered around 0 microns at timepoint 0, indicating that most of the cells were not contracting. As time went on, the distribution of the contraction values shifted toward a higher number, indicating an increase in the average contraction as time progressed. This distribution was not uniform, instead there was significant variability in the contraction values across all timepoints. Interestingly, a small subpopulation of weakly contracting cells was identified in the distribution. Trabecular meshwork cells also contracted on the collagen I micropatterns; however, this contraction was not as robust and was generally more gradual suggesting a slower rate of contraction over time when compared to collagen IV. The cells did not clearly plateau within the 10-hour time frame. As observed with the collagen IV micropatterns, the cells clustered around 0 microns at timepoint 0; however, the distribution of the contraction values on collagen I shifted toward a higher number as time progressed. This suggested an increase in the average contraction of the cells as time progressed albeit it was not as pronounced as it was on collagen IV. The distribution of the contraction values was once again not uniform, instead there was significant variability in the contraction values across all timepoints. A small subpopulation of weakly contractile cells was also observed in the distribution. Interestingly, this small subpopulation was larger on the collagen I micropatterns compared to the collagen IV. While trabecular meshwork cells contracted on the fibronectin micropatterns, the contraction was the least robust and the slowest on this particular protein compared to the other 2 substrates tested. As previously observed with the other 2 substrates tested, the contraction values clustered around 0 microns at timepoint 0. The distribution of the contraction values shifted toward a higher number as time progressed. Interestingly, this shift was significantly less pronounced compared to collagen I and collagen IV micropatterns (**Fig. 6 & 7**).

Discussion

In this section, we aimed to identify the appropriate substrate material for trabecular meshwork cells to exert robust contractile forces. We utilized 96-well FLECS plates containing micropatterns fabricated from collagen I, collagen IV, or fibronectin of equal stiffness, 4-8 kPa, across all 3 plates. Live images of the cell nuclei and micropatterns were captured in parallel every hour for a period of 10 hours under a 5% CO_2 atmosphere at 37°C. In agreement with our previous observations in the pilot experiments, we found that trabecular meshwork cells contracted on all 3 substrates tested. Interestingly, we found that the most robust contraction occurred on the collagen IV micropatterns, followed by collagen I, and finally fibronectin. The cells rapidly and robustly contracted on the collagen IV micropatterns and plateaued at the 6-hour timepoint and stabilized. Trabecular meshwork cells contracted on the collagen I micropatterns; however, the contraction happened much more slowly and was not as robust compared to collagen IV micropatterns. Intriguingly, the slowest and least dramatic contraction occurred on the fibronectin micropatterns. The contraction of the cells on fibronectin was consistently below that of the collagen IV and collagen I micropatterns. The ECM is an intricate network composed of an array of multimodal macromolecules such as collagens, glycoproteins, and proteoglycans. The macromolecules link together covalently or non-covalently to form a structurally stable composite. Evidence has been accumulating to indicate that the ECM is not merely a supporting material for scaffolding of cells. It is also an important factor in the determination of the behavior and biological characteristics of the cells. The ECM components in the trabecular meshwork encompass various types of collagens, proteoglycans, fibronectin, laminin, and elastin. Here, we provide evidence that the ECM substrate on which trabecular meshwork cells attach has a profound effect on their ability to exert contractile forces.

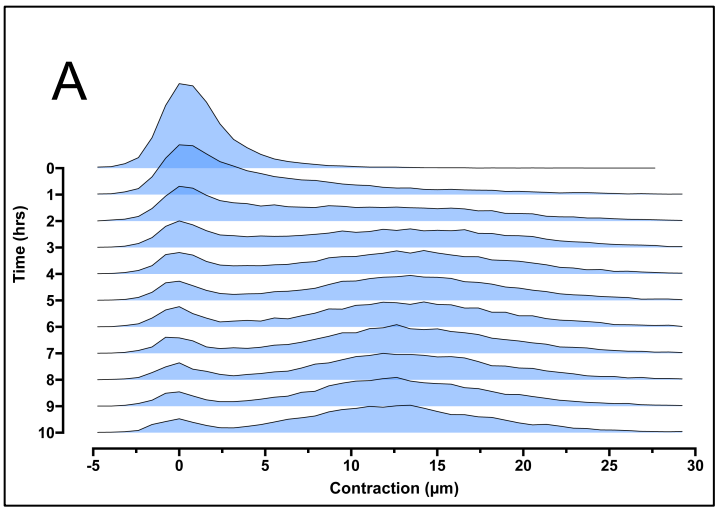
A
Time (hrs)
0
1
2
3
4
5
6
7
8
9
10
-5
0
5
10
15
20
25
30
Contraction (μm)

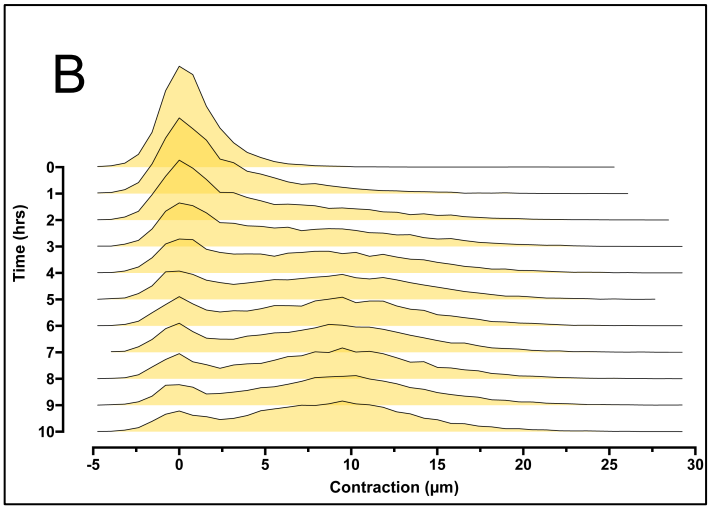
B
Time (hrs)
0
1
2
3
4
5
6
7
8
9
10
-5
0
5
10
15
20
25
30
Contraction (μm)

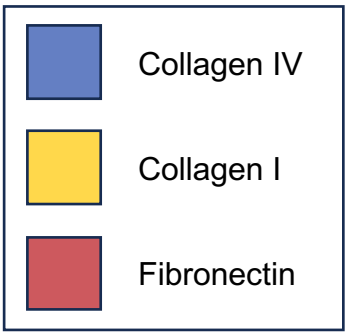
Collagen IV
Collagen I
Fibronectin

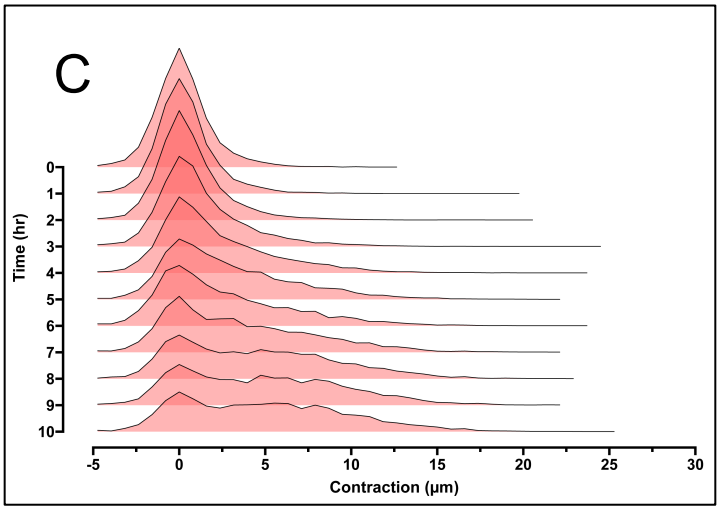
C
Time (hr)
0
1
2
3
4
5
6
7
8
9
10
-5
0
5
10
15
20
25
30
Contraction (μm)

Figure. 6. Distribution of human trabecular meshwork single-cell contractility values on collagen IV, collagen I, or fibronectin substrates. Untreated human trabecular meshwork cells at passage 3 isolated from a single donor (TM408 P1) were seeded on collagen IV, collagen I, or fibronectin micropatterns of 4-8 kPa stiffness. Live images of the cells were taken every-hour for a period of 10-hours. The captured images were analyzed using an image analysis pipeline to obtain single-cell contraction measurements. Each ridge plot contains at least 15,000 single-cell contraction values across all 3 substrates and timepoints. The ridge plots show the time dependent distribution of the single-cell contractility values over a period of 10-hours on collagen IV (A), collagen I (B), or fibronectin (C) micropatterns.

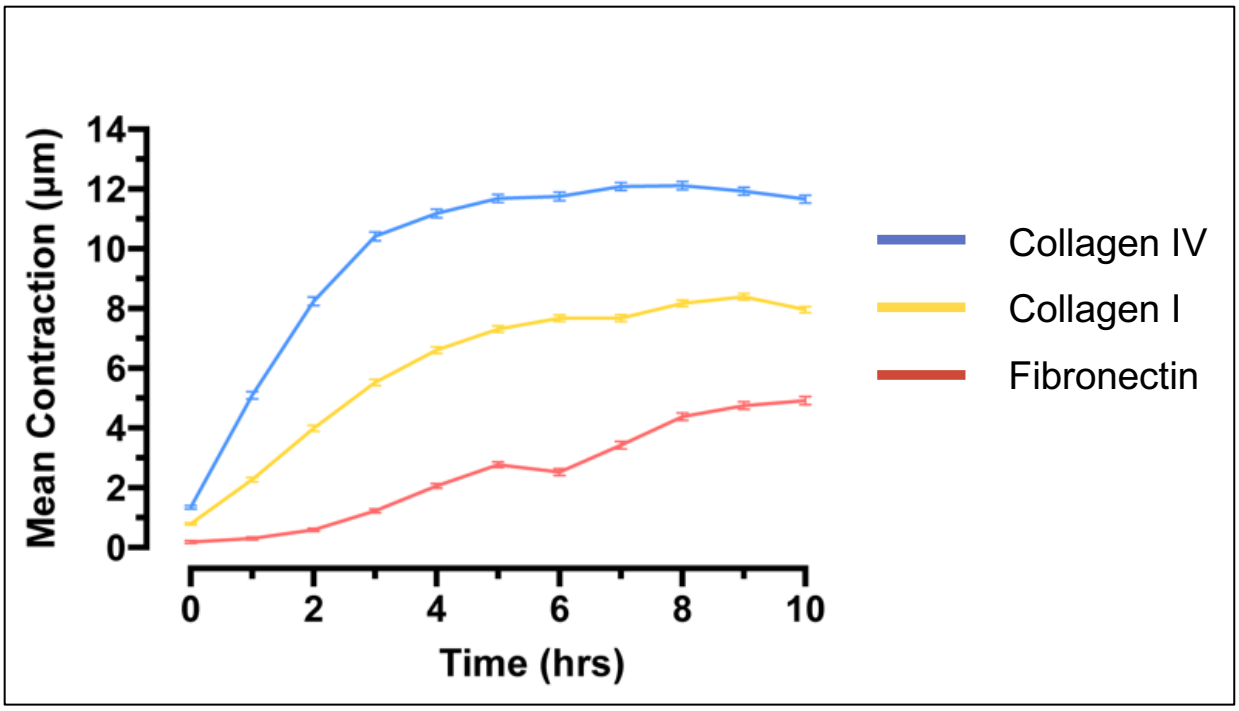

Figure. 7. Effect of substrate material on the contractility of human trabecular meshwork cells at the single-cell level. Untreated trabecular meshwork cells at passage 3 isolated from a single donor (TM408 P1) were seeded on collagen IV, collagen I, or fibronectin micropatterns of 4-8 kPa stiffness. Live images of the cells on the micropatterns were taken every-hour for a period of 10-hours. The captured images were analyzed using an image analysis pipeline to obtain single-cell contraction measurements. Each data point represents the mean of at least 15,000 individual single-cell measurements. Errors bars represent the 95% confidence interval for each data point. The line graphs show the contractile behavior of human trabecular meshwork cells on each ECM substrate material.

Chapter 6: Effects of dexamethasone and substrate stiffness on human trabecular meshwork single-cell contractility

We previously found that trabecular meshwork cells successfully adhered, spread, and remained within 'X'-shaped fluorescent micropatterns featuring a diagonal dimension of 70 μm, and an approximate thickness of 10 μm. A 1:1 seeding ration of cells to micropatterns was determined to be optimal for obtaining the maximal number of single cell attachment. The cells attached to fibronectin, collagen I, and collagen IV micropatterns, consistent with previous studies examining the adhesion of these cells to various extracellular matrix proteins in culture. We also visually determined that the cells preferentially adhered and contracted on stiff rather than soft ECM substrates regardless of the material. Encouraged by these results, we designed an experiment to determine which ECM substrate trabecular meshwork could exert the most robust contractile forces. We found collagen IV micropatterns of a stiffness between 4-8 kPa to be the best substrate for trabecular meshwork cells to exert rapid and robust contractile forces. Having established the optimal conditions to observe robust contractile force generation, we decided to study the effect of dexamethasone on the contractility of trabecular meshwork cells. We also decided to study the contractile properties of dexamethasone treated cells on collagen IV micropatterns of 16-20 kPa, and 40-60 kPa.

Materials and Methods

Taking sterile precautions, a total of 3 96-well FLECS plates fabricated with collagen IV (Cat#96-HC4R-X1-QB12, Cat# 96-HC4R-X1-QC12, Cat# 96-HC4R-X1-QC16), containing approximately 3,200 'X'-shaped fluorescent micropatterns per well, were opened inside a biosafety cabinet. The PBS storage buffer was carefully aspirated from the wells, ensuring the fluorescent micropattern matrix at the well's base was left undisturbed. The wells were washed with 10% FBS TM media to eliminate any potential debris present from the plate fabrication process and to prepare the well

environment for cell introduction. Subsequently, each well in all 3 plates was supplemented with 100 µL of 10% FBS TM media and placed in an incubator at 37°C under a 5% CO_2 atmosphere. Trabecular meshwork cells isolated from 4 different donors were utilized for these experiments. All cells were used at passage 3. The cells were serum starved for 24 hours and then treated with 0.1 µM dexamethasone in serum free media or 0.05% DMSO vehicle control for 5 days. The cells were washed 3 times with PBS, trypsinized for 5 minutes at 37°C, resuspended in 10% FBS TM media, passed through a 40 µm cell strainer, and counted. A total of 3,200 cells were seeded per well in a 100 µL volume of 10% FBS TM media containing 1µg/mL Hoechst 33342 plus 0.1 µM dexamethasone or 0.05% (v/v) DMSO vehicle control. The image acquisition process was performed immediately after a 1-hour incubation at room temperature. Live images of the fluorescent patterns and cell nuclei were obtained using an ImageXpress Micro XL High-Content Imaging System fluorescence microscope at 4X magnification. Live images of the cell nuclei and micropatterns were captured in parallel every hour for a period of 10 hours under a 5% CO_2 atmosphere at 37°C. Image analysis was performed on a pipeline available on Biodock AI.

Results

Trabecular meshwork cells from all donors rapidly and robustly contracted on the 4-8 kPa collagen IV micropatterns consistent with our previous experiments. The next most robust contraction occurred on the 16-20 kPa collagen IV micropatterns, and finally on the 40-60 kPa collagen IV micropatterns. The contraction of the trabecular meshwork cells steadily increased in a time dependent manner and plateaued at the 6-hour time point across all donor cells, treatments, and stiffness levels. Dexamethasone treated trabecular meshwork cells were more contractile across all donors relative to their respective vehicle controls. A significant difference in the contraction of dexamethasone treated trabecular meshwork cells was observed even in the even with increases in stiffness of the collagen IV micropatterns (**Fig. 8**).

Discussion

In this section, we aimed to determine the effect of dexamethasone on the contractility of trabecular meshwork cells. We found that dexamethasone increased the ability of the trabecular meshwork cells to exert strong contractile forces. This result was consistent across all 4 donors tested despite observing donor variability. Interestingly, as the stiffness of the collagen IV micropatterns increased, the overall contraction of the trabecular meshwork cells decreased. While this result was intriguing, it was not entirely surprising since a stiffer matrix is better able to resist deformation compared to a softer matrix. While these results might seem intuitive, the contractile properties of the trabecular meshwork cells have thus far remained incompletely characterized. In addition, the contractility of the trabecular meshwork cells on substrates of varying stiffness has not been thoroughly studies despite stiffness being a critical factor affecting tissue and cell function. It is well established that trabecular meshwork cell contractility is critical for trabecular meshwork tissue function. Previous studies have found that dexamethasone increases the stiffness of trabecular meshwork cells and tissues. Dexamethasone is also known to upregulate the expression of proteins such as α-SMA and phosphorylated-ERK 1/2 associated with the contractile machinery of the trabecular meshwork cells. While numerous studies have provided insights into the molecular mechanisms changes that occur in the trabecular meshwork after prolonged glucocorticoid exposure and varying substrate stiffness, our study provides new evidence support a model where an increase in contractility along with changes in substrate stiffness have a found effect on the functional properties of the trabecular meshwork cells.

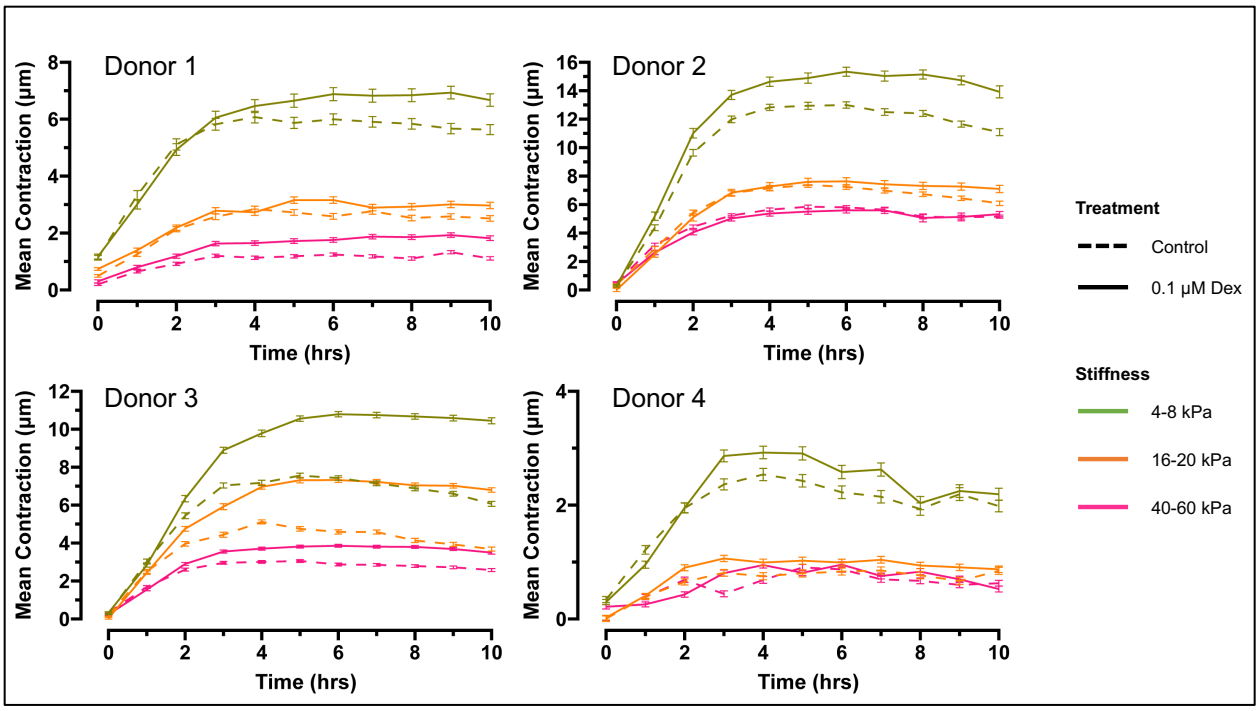

Figure. 8. Dexamethasone induces increased contractility in human trabecular meshwork cells at the single-cell level independent of substrate stiffness. Human trabecular meshwork cells were treated with either control (0.05% DMSO) or 0.1 µM dexamethasone (Dex) over a 5-day period. Following the treatment, the cells were trypsinized and dissociated into single cells in suspension. Subsequently, individual cells were seeded onto collagen IV micropatterns with varying stiffness levels (4-8 kPa, 16-20 kPa, or 40-60 kPa). Live images of the cells on the micropatterns were captured hourly over a 10-hour period. The acquired images underwent analysis through an image analysis pipeline to obtain single-cell contraction measurements. Graphs show representative results across 4 different donors (Donor 1 =TM306, Donor 2 = TM 318, Donor 3 = TM337, & Donor 4= TM340 at P3). Each data point represents the mean of at least 15,000 individual single-cell contraction measurements. Errors bars represent the 95% confidence interval for each data point.

Chapter 7: Effect of actomyosin disruption on human trabecular meshwork single-cell contractility

In the previous chapter, we established the effect of dexamethasone on the contractility of trabecular meshwork cells at the single-cell level. We found that dexamethasone increased the contractility of trabecular meshwork cells. The Rho/ROCK pathway is a master regulator of the actin cytoskeleton and contractility. Previous studies have found that inhibition of this pathway in physiological and pathological states affects the contractility status of the trabecular meshwork at the tissue level. Inhibition of the Rho/ROCK pathway, with agents such as the ROCK inhibitor Y-27632, relaxed the trabecular meshwork tissue, increased outflow facility and lowed intraocular pressure in-vitro and in in-vivo animal models. However, the effect of the ROCK inhibitor Y-27632 on the contractility status of the trabecular meshwork cells at the single-cell level has not been extensively studied. In this chapter, we tested the hypothesis that by inhibiting the Rho/ROCK pathway with the ROCK inhibitor Y-27632 we could decrease the contractility of trabecular meshwork cells.

Materials and Methods

Taking sterile precautions, a 96-well FLECS plates fabricated with collagen IV (Cat#96-HC4R-X1-QB12, 4-8 kPa), containing approximately 3,200 ‘X’-shaped fluorescent micropatterns per well, was opened inside a biosafety cabinet. The PBS storage buffer was carefully aspirated from the wells, ensuring the fluorescent micropattern matrix at the well’s base was left undisturbed. The wells were washed with 10% FBS TM media to eliminate any potential debris present from the plate fabrication process and to prepare the well environment for cell introduction. Subsequently, each well was supplemented with 100 µL of 10% FBS TM media and placed in an incubator at 37°C under a 5% CO_2 atmosphere. Trabecular meshwork cells isolated from 4 different donors were utilized for these experiments. All cells were used at passage 3. The cells

were serum starved for 24 hours prior to treatment with 0.05% DMSO vehicle, 10 μM Y-27632, 0.1 μM dexamethasone, or 10 μM Y-27632 plus 0.1 μM dexamethasone in serum free media for 5 days. The cells were washed 3 times with PBS, trypsinized for 5 minutes at 37°C, resuspended in 10% FBS TM media, passed through a 40 μm cell strainer, and counted. A total of 3,200 cells were seeded per well in a 100 μL volume of 10% FBS TM media containing 1μg/mL Hoechst 33342 plus the respective drug treatments. The image acquisition process was performed immediately after a 1-hour incubation of the plate at room temperature. Live images of the fluorescent patterns and cell nuclei were obtained using an ImageXpress Micro XL High-Content Imaging System fluorescence microscope at 4X magnification. Live images of the cell nuclei and micropatterns were captured in parallel every hour for a period of 10 hours under a 5% CO_2 atmosphere at 37°C. Image analysis was performed on a pipeline available on Biodock AI.

Results

As previously observed, trabecular meshwork cells without any treatment are inherently contractile and displayed a wide range of contractilities which increased in a time dependent manner. Dexamethasone once again increased the contractility of trabecular meshwork cells and also displayed a wide range of contractilities that increased in a time dependent manner. Treatment with the ROCK inhibitor Y-27632 alone inhibited the ability of the majority of trabecular meshwork cells to contract across all timepoints; however, a small sub-population of cells exhibited some degree of contraction. This small sub-population also slightly increased over time. Y-27632 also practically inhibited the overall contractility of dexamethasone treated cells across all timepoints. As observed with the Y-27632 alone groups, there was a small subpopulation of trabecular meshwork cells which exhibited some degree of contraction. This subpopulation was also larger than the subpopulation observed with Y-27632 alone. Intriguingly, the co-treated cells slowly recovered some of their contractile properties as time went on; however, this contraction never reached the heights of the vehicle or dexamethasone treated groups (**Fig. 9**).

Discussion

In this chapter, we performed experiments to study the contractility of trabecular meshwork cells with inhibition of the Rho/ROCK pathway in an in vitro model of chronic steroid exposure. Previous studies have found that inhibition of this pathway in physiological and pathological states affects the contractility status of the trabecular meshwork at the tissue level. Inhibition of the Rho/ROCK pathway, with agents such as the ROCK inhibitor Y-27632, relaxed the trabecular meshwork tissue, increased outflow facility in human ex-vivo perfusion eye systems and lowed intraocular pressure in in-vivo animal models. Y-27632 is widely used as a specific inhibitor of the Rho-associated coiled-coil forming protein serine/threonine kinase (ROCK) family of protein kinases, which include ROCK1 and ROCK2. Y-27632 inhibits ROCK1 and ROCK2 by competing with ATP for binding to the kinases. The ROCK family of kinases are downstream effectors of Rho, a member of the Rho family of GTPases which include RhoA, RhoB, and RhoC. The Rho/ROCK pathway plays a critical role in the formation of actin stress fibers, focal adhesions, and the downregulation of myosin phosphatase. Thus, the Rho/ROCK pathway is a master regulator of the actin cytoskeleton and cell contractility. Previous studies have shown that the glucocorticoid dexamethasone increases the expression and transiently activates RhoA in human trabecular meshwork cells, which further activated the downstream effector ROCK. In addition, human trabecular meshwork cells expressing a constitutively activated form of RhoA (RhoAV14) exhibited increased F-actin, vinculin, and MLC phosphorylation as well as increased levels of fibronectin, laminin, tenascin C, and α-SMA all which have been associated with a contractile phenotype. These dexamethasone-induced effects have also been successfully inhibited by treatment with Y-27632. Nevertheless, quantitative evidence showing a decreased in cellular force generation at the single-cell level in dexamethasone treated cells after treatment with Y-27632 is lacking. To address this gap in our knowledge, we treated primary human trabecular meshwork cells with either vehicle control, Y-27623, dexamethasone, and dexamethasone plus

Y-27632 and employed our optimized FLECS contractility assay to quantitatively measure the contraction of the cells in a time dependent manner. We found that Y-27632 inhibited the contractility of control and dexamethasone treated cells in practically all cells with the exception of small subpopulations which still displayed some degree of contraction. These results seem to agree with previous observations using the bulk contractility assay which showed that Y-27632 inhibits the contraction of collagen gels containing trabecular meshwork cells. The collagen gels also recovered some degree of contraction as time went on. However, in our study we can observed this recovery in contraction is most likely due to a sub-population of highly contractile cells previously unidentified by the bulk contractility assay.

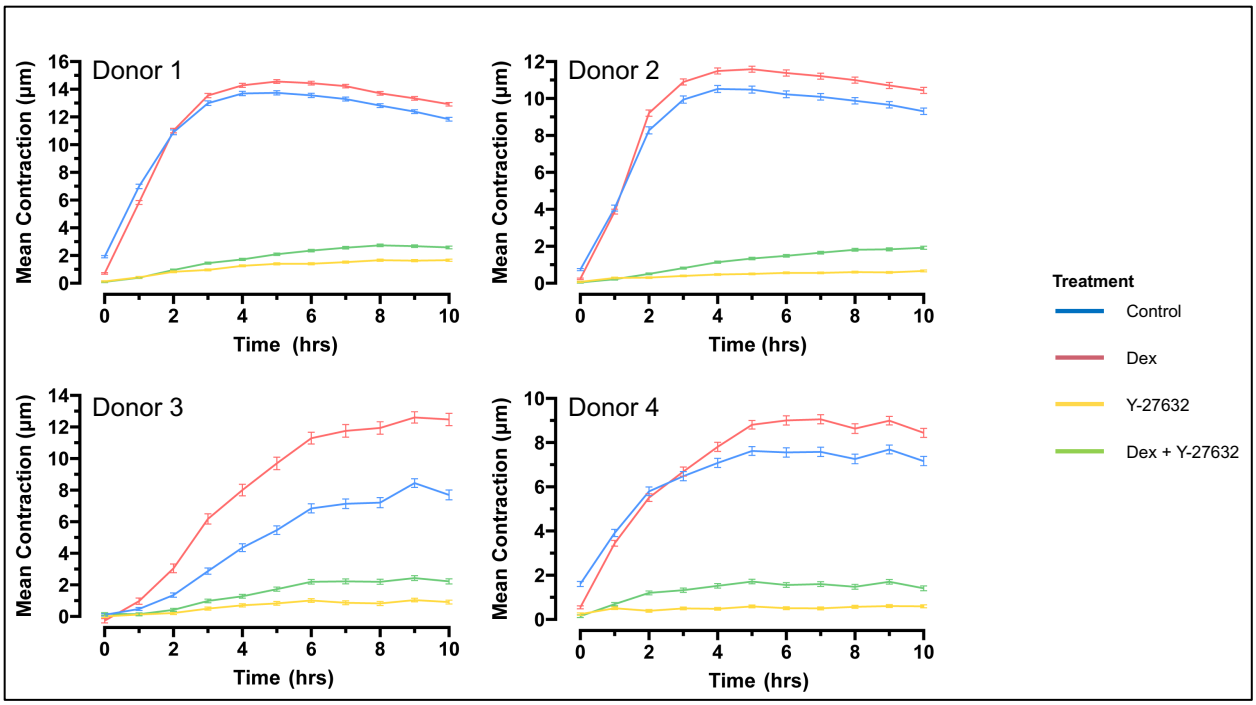

Figure. 9. The ROCK inhibitor Y-27632 inhibits normal and dexamethasone induced contraction of human trabecular meshwork cells at the single-cell level. Human trabecular meshwork cells were treated with control (0.05% DMSO) ,0.1 µM dexamethasone (Dex), 10 µM Y-27632 ROCK inhibitor, or 10 µM Y-27632 ROCK inhibitor and 0.1 µM dexamethasone (Dex) for 5-days. Following treatment, trabecular meshwork cells were trypsinized, dissociated into single cells in suspension, and subsequently seeded onto collagen IV micropatterns of a stiffness of 4-8 kPa. Live images of individual cells on the micropatterns were captured hourly over a 10-hour period. The acquired images underwent analysis through an image analysis pipeline to obtain single-cell contraction measurements. Graphs present representative results across 4 different donors (Donor 1= TM349, Donor 2= TM402, Donor 3 = TM403, & Donor 4= TM405 at P3). Each data point represents the mean of at least 15,000 individual single-cell measurements. Errors bars represent the 95% confidence interval for each data point.

CHAPTER 8: Conclusion

In conclusion, this thesis aimed to characterize the contractile properties of human trabecular meshwork cells in normal and in an in-vitro model of chronic steroid exposure at the single-cell level. The documented prevalence of elevated intraocular pressure in a significant proportion of the population underscores the urgency of understanding the underlying mechanisms leading to this condition, which may result in steroid-induced glaucoma. The elucidation of molecular changes within the trabecular meshwork due to prolonged steroid exposure, encompassing alterations in extracellular matrix metabolism, cytoskeletal organization, and gene expression, forms the foundation of this investigation. Despite these molecular insights, a notable gap exists in understanding the specific functional changes occurring at the cellular level, prompting the adaptation and optimization of the Fluorescently Labeled Elastomeric Contractible Surfaces (FLECS) assay. The FLECS assay, introduced in this thesis, emerges as a versatile tool capable of providing detailed contractility measurements at the single-cell level on substrates with tunable stiffness. This novel tool has enabled the presentation, for the first time, of single-cell-level contractile variations in human trabecular meshwork cells under primary culture conditions and in an in vitro model simulating chronic steroid exposure. Significantly, the findings from this research reveal that increased contractility, coupled with modifications in extracellular matrix components, cytoskeletal organization, and stiffness, may collectively contribute to the elevation of intraocular pressure. These insights contribute substantially to our understanding of the pathophysiological processes underlying steroid-induced ocular hypertension and its potential progression to permanent vision loss through steroid-induced glaucoma. As we navigate the nuanced interplay between cellular contractility and molecular alterations, this study not only addresses the immediate need for a comprehensive evaluation of trabecular meshwork function but also sets the stage for future investigations. These may include exploring targeted interventions or therapeutic strategies aimed at mitigating the adverse effects of prolonged steroid exposure on

ocular health. In essence, this thesis provides a valuable contribution to the scientific understanding of steroid-induced ocular hypertension, offering insights that may inform both clinical practice and future research endeavors in ophthalmology.

Appendix

Experimental Eye Research 214 (2022) 108888

Contents lists available at ScienceDirect

Experimental Eye Research

journal homepage: www.elsevier.com/locate/yexer

Characterizing the metabolic profile of dexamethasone treated human trabecular meshwork cells

Kimberly Graybeal [a], Luis Sanchez [a], Chi Zhang [a], Linsey Stiles [b], Jie J. Zheng [a,*]

[a] Stein Eye Institute, Department of Ophthalmology, David Geffen School of Medicine, The Molecular Biology Institute at the University of California, Los Angeles, Los Angeles, CA, USA
[b] Department of Medicine, Department of Molecular and Medical Pharmacology, David Geffen School of Medicine, University of California, Endocrinology, Los Angeles, CA, USA

ARTICLE INFO

Keywords:
Trabecular meshwork
Primary open angle glaucoma
Myocilin
Mitochondria

ABSTRACT

The trabecular meshwork (TM) is the leading site of aqueous humor outflow in the eye and plays a critical role in maintaining normal intraocular pressure. When the TM fails to maintain normal intraocular pressure, glaucoma may develop. Mitochondrial damage has previously been found in glaucomatous TM cells; however, the precise metabolic activity of glaucomatous TM cells has yet to be quantitatively assessed. Using dexamethasone (Dex) treated primary human TM cells to model glaucomatous TM cells, we measure the respiratory and glycolytic activity of Dex-treated TM cells with an extracellular flux assay. We found that Dex-treated TM cells had quantifiably altered metabolic profiles, including increased spare respiratory capacity and ATP production rate from oxidative phosphorylation. Therefore, we propose that reversing or preventing these metabolic changes may represent an avenue for future research.

Elevated intraocular pressure (IOP) is a primary risk factor for the development of glaucoma, a leading cause of irreversible blindness that affects over 70 million people across the world, with primary open-angle glaucoma (POAG) being the most common form. (Braunger et al., 2015; Caprioli, 2013; Quigley, 2011; Tham et al., 2014). The trabecular meshwork (TM), which maintains IOP homeostasis by generating resistance to aqueous humor outflow, is a crucial part of this mechanism (Braunger et al., 2015; Gasiorowski and Russell, 2009; Stothert et al., 2016; Xie et al., 2019). The TM is a complex, filter-like structure of connective tissue consisting of beams and sheets of extracellular matrix surrounded by TM cells that resides in the iridocorneal angle of the eye (Stamer and Clark, 2017). After aqueous humor is produced in the ciliary body, it travels through the pupil, into the anterior chamber, and exits into the Schlemm's canal through the TM (Carreon et al., 2017; Roy Chowdhury et al., 2015). When the TM fails to maintain adequate outflow, POAG can develop: increased outflow resistance in the TM drives increased IOP, which can damage the optic nerve and lead to vision loss (Caprioli, 2013; Kwon et al., 2009).

Glucocorticoids, such as Dexamethasone (Dex), are used clinically to decrease inflammation, but use in the eye can increase outflow resistance in the TM and therefore elevate IOP (Fini et al., 2017). Because similar changes occur in POAG TM, glucocorticoid-treated TM cells are viewed as an *in vitro* model system (Gasiorowski and Russell, 2009; Tamm, 2002; Wordinger and Clark, 1999). A hallmark of Dex-treated TM cells is the upregulation of myocilin, a protein also linked to glaucoma pathogenesis (Gasiorowski and Russell, 2009; Kwon et al., 2009). Previous studies have shown that myocilin localizes to the mitochondria, where it may have pro-apoptotic effects including reducing membrane potential (Sakai et al., 2007; Stothert et al., 2016; Wentz-Hunter et al., 2002). Furthermore, mitochondrial damage has been observed in the TM of patients with glaucoma (Izzotti et al., 2010). Given this association between POAG pathogenesis and TM mitochondria, we decided to characterize the metabolic profile of Dex-treated primary human TM cells. We employed extracellular flux (XF) analysis to quantify metabolic activity at the cellular level by measuring the oxygen consumption rate (OCR) and the extracellular acidification rate (ECAR).

In the study, we used four TM tissues obtained from four independent donors. The first TM (TM 223) was from a 70-year-old female donor. The second TM (TM 248A) was from a 67-year-old Caucasian female donor. The third TM (TM 301) was from a 60-year-old Caucasian male donor. The fourth TM (TM 303) was from a 68-year-old Asian male donor. TM cells were isolated from tissue using blunt dissection and plated on 6-

* Corresponding author. Stein Eye Institute, Department of Ophthalmology, David Geffen School of Medicine at UCLA, 100 Stein Plaza, Los Angeles, CA, 90095, USA.
E-mail address: jzheng@jsei.ucla.edu (J.J. Zheng).

https://doi.org/10.1016/j.exer.2021.108888
Received 9 August 2021; Received in revised form 29 November 2021; Accepted 3 December 2021
Available online 9 December 2021

well plates coated with 0.5% filtered gelatin in water. The TM cells were cultured in Dulbecco's Modified Eagle's Medium (DMEM) with GlutaMAX containing 1 g/L D-glucose, 110 mg/L Sodium Pyruvate, 10% Fetal Bovine Serum (FBS), and 1% 100x Antibiotic-Antimycotic or Penicillin-Streptomycin (Keller et al., 2018). The medium was changed every 2–3 days. Once confluency was reached, the cells were passaged to a new plate. Medium was removed and the cells were rinsed three times with Dulbecco's phosphate-buffered saline (DPBS). Enough 0.25% trypsin with ethylenediaminetetraacetic acid (EDTA) was added to cover the wells, and the cells were incubated at 37 °C and 5% CO_2 for 5 mins. Medium was added to neutralize trypsin and cells were resuspended and placed in a new gelatin-coated container. Cells were allowed 24 h to adhere, and regular culturing methods were resumed.

The four TM cells, TM 223, TM 248A, TM 301 and TM 303, had spindle-like, fibroblastic morphology (Fig. 1A–D), matching previous descriptions (Keller et al., 2018; Stamer and Clark, 2017). As Dex-induced myocilin expression is the principal marker for TM cells (Gasiorowski and Russell, 2009), we used qPCR to conduct further validation. Treatments of the TM cells with Dex were started after the cells reached confluence. Half of the wells were treated with 100 nM Dex dissolved in dimethyl sulfoxide (DMSO) and the other half acted as the vehicle control. Medium with Dex or vehicle was changed daily for five days. Following five-day Dex treatment, total cellular RNA was extracted from TM cells using the Qiagen RNeasy mini kit (Qiagen, Valencia, CA) as per manufacturer's protocol. The concentration of RNA was analyzed using a NanoDrop 2000 (ThermoFisher, Waltham, MA) and the quality of the RNA was determined on the ratio of absorbance at 260 nm and 280 nm. Quantitative PCR was accomplished using qScript-XLT 1-Step RT-qPCR kit from Quanta Biosciences (Beverly, MA) per manufacturer's instructions on a Realplex 2 (Eppendorf, Hauppauge, NY) with TaqMan primers for human *GAPDH* (Hs02758991_g1) and human *MYOC* (Hs00165345_m1) purchased from ThermoFisher Scientific (Canoga Park. CA). *GAPDH*-normalized *MYOC* fold changes of each TMs were determined by the Delta-Delta Ct method. We found that Dex increased *MYOC* expression by 10.1 ± 0.1 fold (TM 223), 19.8 ± 0.1 fold (TM 248A), 17.2 ± 0.4 fold (TM 301), and 19.0 ± 0.6 fold (TM 303) (data not shown), confirming that all four cells are TM cells.

For the extracellular flux analysis, we utilized the Seahorse XF96 Flux Analyzer and performed the Mito Stress Test (Zhang and Zhang, 2019), which took 70–104 min. The Mito Stress Test includes sequential injection of the ATP Synthase inhibitor oligomycin, the chemical uncoupler carbonyl cyanide-p-trifluoromethoxyphenylhydrazone (FCCP), and the Complex I and III inhibitors rotenone and antimycin A. Six main parameters are determined by oxygen consumption rate (OCR) analysis: basal respiration, ATP-linked respiration, proton leak, maximal respiration, spare respiratory capacity (SRC), and non-mitochondrial respiration. Basal respiration provides information on respiration driven by ATP synthesis (ATP demand) and proton leak in the cell. The addition of oligomycin will decrease respiration that is coupled to ATP synthesis (ATP-linked respiration). The remaining respiration is due to proton leak (dissipation of the gradient through other means than ATPase) and can be used to calculate ATP-linked respiration (basal OCR – proton leak). FCCP, a protonophore uncoupler, is then added to induce maximal respiration by dissipating the proton gradient created by the ETC. Maximal respiration is calculated as the highest OCR after injection of FCCP. Lastly, antimycin-A, a complex III inhibitor, and rotenone, a complex I inhibitor, halt ETC activity altogether, thereby halting all mitochondrial oxygen consumption. The remaining OCR level represents the non-mitochondrial oxygen consumption, which is subtracted from the other measurements before analysis. Finally, the difference between maximal and basal respiration represents the spare respiratory capacity, also called reserve capacity, which can indicate a cell's ability to respond to increased energy demands. This is demonstrated schematically in Fig. 1I. ATP production rate can be defined as mitochondrial (produced through oxidative phosphorylation, or OxPhos) or glycolytic, produced through glycolysis. ATP production rate was calculated as

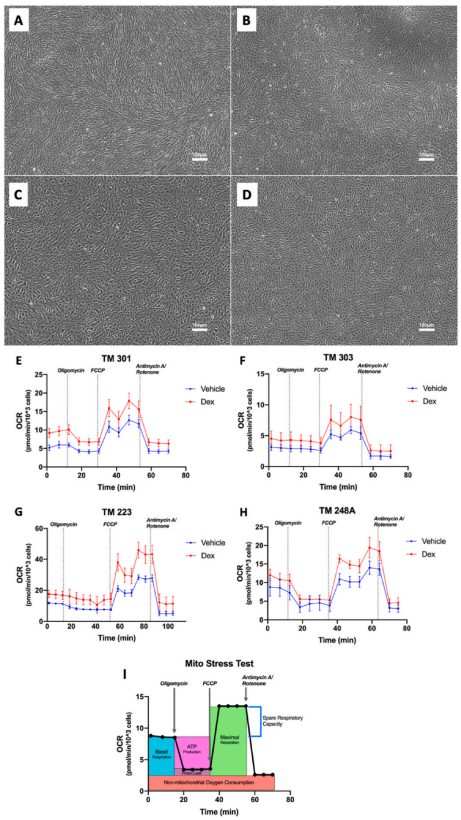

Fig. 1. Cell imaging of four human TM samples used in the study (A–D) and the oxygen consumption rates (OCRs) of the four cells during the Seahorse extracellular flux (XF) measurement (E–H). Schematic diagram of typical XF trace, demonstrating how each parameter is determined (I).
(A) TM 303 cells at passage 1; (B) TM 301 cells at passage 1; TM 223 cells at passage 1 (C); and TM 248A cells at passage 1 (D). Before being analyzed with the XF Cell Mito Stress Test assay, the cells were treated with 100 nM Dex or vehicle DSMO for five days. The OCRs of the four cells (E–H) were measured throughout injections of four compounds (2.0 μM oligomycin, 0.75 μM FCCP, 2.0 μM Antimycin-A and 2.0 μM rotenone), and the dotted lines indicate injection times. (E) TM 301 cells; (F) TM 303 cells; (G) TM 223 cells; and (H) TM 248A cells. Each data point of E-H summarizes 4–5 technical replicates of a single experiment. Error bars reflect standard deviation of those technical replicates.

described by Divakaruni et al. (2017). ECAR is simultaneously measured (traces not shown) and can be used to calculate basal ECAR, ECAR levels before compound addition, and glycolytic reserve, which is similar to spare respiratory capacity, but for glycolysis. Glycolytic reserve indicates ability to increase glycolytic activity in response to demand or the closeness of a cell's glycolytic flux to its maximum (Divakaruni et al., 2014).

Two central cellular processes to produce energy as ATP are aerobic

respiration and anaerobic glycolysis (Green et al., 2014). In aerobic respiration, which occurs in the mitochondria, the majority of ATP is made through OxPhos that consumes oxygen in the process. The change in extracellular oxygen concentration is measured as the OCR, which we use as a proxy for mitochondrial respiratory activity (Zhang and Zhang, 2019). ATP can also be made through anaerobic glycolysis, a process which ultimately produces protons ($lactate^- + H^+$). These protons acidify the surrounding media and are measured as ECAR, a proxy for glycolytic activity. Oxygen is not consumed by anerobic glycolysis. Thus, by utilizing XF analysis of OCR and ECAR in this study, we quantify the effect of Dex-treatment on the metabolism of TM cells.

For the XF measurement, each cell strain was at passage three. TM cells were plated and treated on a Seahorse XF analyzer 96-well microplate. Cells were not plated on the outer ring of the 96-well plate to avoid edge effects. Four experiments were performed on different days, one for each sample tissue, with each culture plated in 4–5 technical replicates. The assay was prepared according to established procedure (Divakaruni et al., 2014). On the day of the assay, the cells were washed twice to replace growth medium with DMEM assay medium consisting of 10 mM glucose, 2 mM glutamine, 1 mM pyruvate, and 5 mM HEPES. A cartridge with O_2 and pH fluorophore sensors was hydrated overnight and calibrated before the cell plate was inserted into the Seahorse XF96 Flux Analyzer. The cells were washed twice with assay medium, removing the Dex and incubated for 30 min before starting the assay. During each measurement, the cartridge created a 2.28 μL transient microchamber where changes in oxygen concentration and pH were measured in real time. OCR and the ECAR were measured during injections of four compounds: 2.0 μM oligomycin, 0.75 μM FCCP injected in Ports B and C (final concentration of 0.75 μM and 1.35 μM FCCP respectively), and 2.0 μM Antimycin-A and 2.0 μM rotenone, which were added simultaneously. FCCP was injected twice to ensure that maximal respiration was achieved during the assay. Oxygen consumption was normalized to cell number per well after the assay and OCR is reported in pmol O_2 per minute per 10^3 cells. Cell number per well was quantified by staining the cells with Hoechst in the XF96 microplate and counting nuclei with an Operetta High Content Imaging System (PerkinElmer). Raw OCR traces for each sample are shown in Fig. 1E–H.

Results from the Mito Stress Test demonstrate that while basal respiration was not consistently affected (n = 4, ns) (Fig. 2A), Dex-treated cells had maximal respiration values 1.36 ± 0.082 times higher than vehicle cells (n = 4, P < 0.001) (Fig. 2B) and SRC values 1.41 ± 0.18 times larger than vehicle cells (n = 4, P < 0.001) (Fig. 2C). ATP-linked respiration was 1.50 ± 0.36 times higher in Dex-treated cells than in vehicle cells (Fig. 2E). Non-mitochondrial oxygen consumption was also 1.73 ± 0.38 times larger than vehicle cells (n = 4, P < 0.05) (Fig. 2F). ATP production rates from OxPhos increased in Dex-treated cells by 1.48 ± 0.34 fold (n = 4, P < 0.05) (Fig. 2D), and the proportion of ATP production from OxPhos out of total ATP production rate was higher in Dex-treated cells, by 1.31 ± 0.14 fold (n = 4, P < 0.05) (Fig. 2K). In vehicle cells, ATP production rate from OxPhos made up an average 24.5% of total ATP production rate, compared to 32.4% in Dex-treated cells (n = 4, ns) (Fig. 2J). ATP production rate from glycolysis represented 75.5% of total ATP production rate in vehicle cells, versus

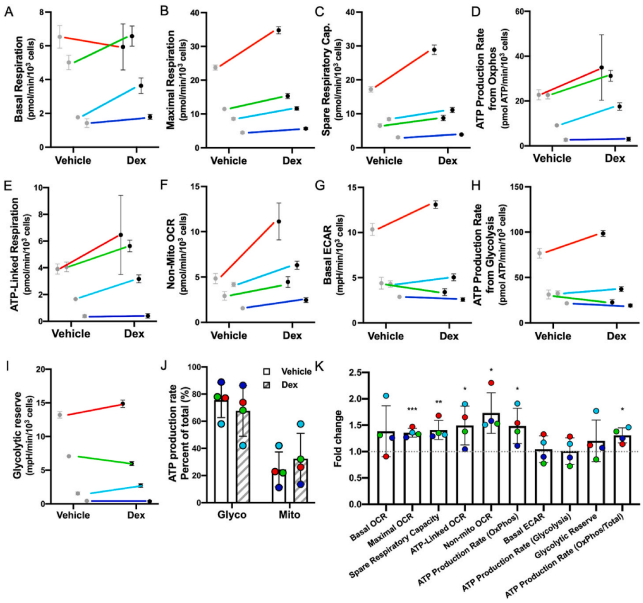

Fig. 2. Data calculated from the XF analysis. A-J reflect the raw OCR and ECAR data for each parameter and sample. K is a summary diagram demonstrating the fold change and significance values for each parameter. Dex did not significantly or consistently affect basal respiration (n = 4, ns) (A), but Dex-treated cells had increased maximal respiration (n = 4, P < 0.001) (B), spare respiratory capacity (n = 4, P < 0.01) (C), ATP production rate from OxPhos (n = 4, P < 0.05) (D), ATP-linked respiration (n = 4, P < 0.05) (E), and non-mitochondrial oxygen consumption (n = 4, P < 0.05) (F) compared to vehicle cells. Glycolytic properties, basal ECAR (n = 4, ns) (G), ATP production rate from glycolysis (n = 4, ns) (H), and glycolytic reserve (n = 4, ns) (I), were not significantly or consistently affected. The share of total ATP production from OxPhos was increased in Dex cells while the share of ATP production from glycolysis was decreased (n = 4, ns) (J). These changes were consistent between each strain but not statistically significant. K summarizes the fold change significance data for parameters A-I as well as the proportion of ATP production rate from OxPhos out of total, which was increased in Dex-treated cells (n = 4, P < 0.05) (K). Each data point is the average fold change of Dex-treated cells compared to vehicle cells which were normalized to one, as represented by the dotted line. TM223 is colored red, TM248A is green, TM 301 is light blue, and TM 303 is dark blue.
(*) indicates p < 0.05. (**) indicates p < 0.01. (***) indicates p < 0.001. Each data point summarizes 4–5 technical replicates of a single experiment. Error bars in A-I reflect standard deviation of those technical replicates. Error bars in J-K reflect standard deviation of the means of each sample's technical replicates. Significance was determined with a standard two-tailed T test using fold change data. (For interpretation of the references to color in this figure legend, the reader is referred to the Web version of this article.)

67.6% in Dex-treated cells (n = 4, ns) (Fig. 2J). Analysis of ECAR reveals that Dex did not have a significant effect on trends of other glycolytic properties, such as glycolytic reserve, basal ECAR, and ATP production rate from glycolysis (n = 4) (Fig. 2G–I). Significance was determined with a standard two-tailed T-test using fold change data. Each data point summarizes 4–5 technical replicates of a single experiment. Error bars in Fig. 2A–I reflect the standard deviation of those technical replicates. Error bars in Fig. 2J–K reflect the standard deviation of the means of each sample's technical replicates.

As showed in Fig. 1F, TM 303 cells lacked a response to oligomycin. Since TM 303 cells were otherwise consistent with the other TM cells we studied, the lack of oligomycin response is likely due to a technical error, not a biological nonresponse. Nevertheless, this affects parameters requiring oligomycin to calculate, such as ATP-linked respiration, ATP production rate from OxPhos, and glycolytic reserve, for which TM 303 cells values changed very little (Fig. 2D, E and 2J, 2I, respectively). When data from TM 303 cells were omitted from the analysis, ATP-linked respiration increased by 1.65 ± 0.26 fold in Dex-treated cells (n = 3, $P < 0.05$), and ATP production rate from OxPhos increased by 1.61 ± 0.28 fold in Dex-treated cells (n = 3, $P < 0.05$). ATP production rate from OxPhos made up an average of 29.0% of the total ATP production rate, compared to 38.7% in Dex-treated cells (n = 3, ns). ATP production rate from glycolysis represented 71.0% of the total ATP production rate in vehicle-treated cells versus 61.3% in Dex-treated cells (n = 3, ns).

In our study, we observed consistent results in primary TM cells from independent donors that Dex-treated cells had increased maximal respiration, SRC, ATP-linked respiration, and non-mitochondrial respiration (Fig. 2B, C, E, F, respectively), while basal respiration was not significantly affected (Fig. 2A). Furthermore, Dex increased ATP production rates from OxPhos (Fig. 2D) and increased the proportion of total ATP production coming from OxPhos (Fig. 2K).

The Dex-treated cells had a measurable increase in the proportion of total ATP production that came from OxPhos: when the data of TM 303 cell is omitted, 29% of total ATP production came from OxPhos in vehicle-treated cells versus an average of 39% in Dex-treated cells (Fig. 2J). With the data of TM 303, 24.5% of total ATP production came from OxPhos in vehicle-treated cells, compared to 32.4% in Dex-treated cells (Fig. 2J). Although these numbers are not statistically significant due to limited number of cell strains used in the study, the trend is significant: in each cell strain, Dex increased the proportion of total ATP production rate from to OxPhos by an average 31% (n = 4, $p < 0.05$) (Fig. 2J). Previously, it was estimated that in TM tissue, approximately three quarters of ATP production come from glycolysis and one quarter from respiration (Epstein and Anderson, 1981), and this aligns well with our data that 24.5% of ATP production in vehicle cells was produced by OxPhos (Fig. 2J). Thus, the increase in Dex-treated cells from the standard average 24.5%–32.4% is a departure from the TM cells' normal metabolic state. Nonetheless, glycolysis remained the dominant source of ATP production in both cases, with 75.5% of ATP production from glycolysis in vehicle cells and 67.6 in Dex-treated cells (Fig. 2J), and the difference was not statistically significant. Given that TM cells reside in a largely low-oxygen environment within the eye (Beebe et al., 2014), it is not surprising that overall TM cells may rely more so on glycolysis for energy. Still, while the majority of energy utilized by TM cells appears to come from glycolysis, our data suggests Dex-treated cells depend more than untreated cells on OxPhos, also exemplified by the statistically significant increase in ATP-linked respiration (Fig. 2E). The lack of a significant and consistent effect on glycolytic properties (Fig. 2G–I) suggests Dex may not be significantly influencing the glycolytic pathway in these cells.

Both Dex-treated TM cells express higher levels of extracellular matrix proteins, including fibronectin, collagen, and laminin (Stamer and Clark, 2017) and therefore may require additional energy to drive this increase in transcription and translation. Increased respiratory capacity and ATP-linked respiration, as observed here, may occur to accommodate these needs. Additionally, it is known that oxidative phosphorylation produces more ATP per glucose molecule than glycolysis, up to 32 versus net 2 ATP, so an increase in energy demand to support extracellular matrix protein production may also explain Dex-treated cells' increased dependence on OxPhos for ATP production. Of note, when TM-1 cells, an immortalized TM cell line that does not upregulate myocilin upon glucocorticoid treatment (Filla et al., 2011), were treated with Dex, none of the tested parameters were significantly affected in two separate experiments (data not shown). This data further supports upregulation of myocilin as an influential factor since TM-1 cells lost some biological properties of TM cells (Gasiorowski and Russell, 2009; Keller et al., 2018).

The increase in ATP-production from OxPhos may also be connected to increased mitochondrial content and number in Dex-treated TM cells. Animal studies have found that Dex-treated mouse and bovine TM cells have more mitochondria per cell, as well as more organelles involved in protein synthesis such as endoplasmic reticula and ribosomes (Sibayan et al., 1998; Zeng et al., 2020). POAG human TM cells have significantly higher ratios of mtDNA to nuclear DNA (nDNA), indicating more mitochondria per cell (Izzotti et al., 2010). Additionally, Dex-treated mouse TM cells have larger mitochondria (Zeng, 2020) and therefore potentially larger cristae, which may translate to more space for OxPhos to occur (Javadov 2018). These morphological changes could also be the cause of the observed Dex-induced increases in maximal respiration and SRC.

The Dex-induced increases in ATP production rate observed in this study may elevate levels of reactive oxygen species (ROS) in the TM. Mitochondria are one of the largest sources of ROS, and ROS are produced in the mitochondria mainly during OxPhos through the oxidation of nicotinamide adenine dinucleotide (NADH) (Izzotti et al., 2010; Sacca et al., 2015). This is consistent with our observation that the Dex-treated TM cells had larger non-mitochondrial oxygen consumption rates (Fig. 2F) which indicates higher levels of ROS production (Wang et al., 2018). Indeed, glaucomatous and Dex-treated TM cells are known to possess higher ROS levels (He et al., 2008; Izzotti et al., 2010; Sacca et al., 2015).

ROS have been recognized to play an important role in the development of glaucoma (Izzotti et al., 2010; Sacca et al., 2005). Both ROS production and damage of ROS to TM cells are linked to mitochondrial activity (He et al., 2008). Long-term ROS exposure contributes to apoptosis and mitochondrial damage (Izzotti et al., 2010), as well as decreased aqueous humor outflow at the TM (Gasiorowski and Russell, 2009) and ultimately ocular hypertension and glaucoma pathogenesis (Sacca et al., 2005). In the current study, we did not observe in the extracellular flux analysis symptoms of mitochondrial damage that may be expected from ROS in the Dex-treated TM cells. It is likely that the five-day Dex treatment may be not long enough to cause mitochondrial damage. Nonetheless, sustained increased demand on the mitochondria, as was observed in this study, especially in the low oxygen environment of the TM, may ultimately result in mitochondrial dysfunction and thus contribute to increased outflow resistance seen in Dex-treated TM. Indeed, the TM cells of POAG patients possess traits indicative of mitochondrial dysfunction, including higher levels of endogenous ROS, decreased membrane potentials, and increased sensitivity to complex I inhibition and other secondary stressors (He et al., 2008). In addition, mtDNA is particularly susceptible to oxidative stress, and, accordingly, increased incidence of the $mtDNA^{4977}$ deletion is a form of mitochondrial damage found in POAG patients (Izzotti et al., 2010; Yusoff et al., 2019). Mitochondrial dysfunction such as these in turn lead to a further increase in ROS levels (Sacca et al., 2015) and further cell death, thus perpetuating a cycle of damage. Given the havoc ROS can wreak on TM cells, the metabolic changes induced by Dex treatment may therefore be one causative factor for the development of glaucoma-like symptoms in Dex-treated TM, including mitochondrial damage and cell death.

Acknowledgements

We thank Dr. Donna Peters for providing TM-1 cells. This study was supported in part by NIH grants R01EY028557 and by Research to Prevent Blindness.

References

Beebe, D.C., Shui, Y.B., Siegfried, C.J., Holekamp, N.M., Bai, F., 2014. Preserve the (intraocular) environment: the importance of maintaining normal oxygen gradients in the eye. Jpn. J. Ophthalmol. 58, 225–231.

Braunger, B.M., Fuchshofer, R., Tamm, E.R., 2015. The aqueous humor outflow pathways in glaucoma: a unifying concept of disease mechanisms and causative treatment. Eur. J. Pharm. Biopharm. 95, 173–181.

Caprioli, J., 2013. Glaucoma: a disease of early cellular senescence. Invest. Ophthalmol. Vis. Sci. 54, ORSF60–67.

Carreon, T., van der Merwe, E., Fellman, R.L., Johnstone, M., Bhattacharya, S.K., 2017. Aqueous outflow - a continuum from trabecular meshwork to episcleral veins. Prog. Retin. Eye Res. 57, 108–133.

Divakaruni, A.S., Paradyse, A., Ferrick, D.A., Murphy, A.N., Jastroch, M., 2014. Analysis and interpretation of microplate-based oxygen consumption and pH data. Methods Enzymol. 547, 309–354.

Divakaruni, A.S., Wallace, M., Buren, C., Martyniuk, K., Andreyev, A.Y., Li, E., Fields, J. A., Cordes, T., Reynolds, I.J., Bloodgood, B.L., Raymond, L.A., Metallo, C.M., Murphy, A.N., 2017. Inhibition of the mitochondrial pyruvate carrier protects from excitotoxic neuronal death. J. Cell Biol. 216, 1091–1105.

Epstein, D.L., Anderson, P.J., 1981. In vitro biochemistry of trabecular meshwork. Vis. Res. 21, 161.

Filla, M.S., Schwinn, M.K., Nosie, A.K., Clark, R.W., Peters, D.M., 2011. Dexamethasone-associated cross-linked actin network formation in human trabecular meshwork cells involves beta 3 integrin signaling. Invest. Ophthalmol. Vis. Sci. 52, 2952–2959.

Fini, M.E., Schwartz, S.G., Gao, X., Jeong, S., Patel, N., Itakura, T., Price, M.O., Price Jr., F.W., Varma, R., Stamer, W.D., 2017. Steroid-induced ocular hypertension/glaucoma: focus on pharmacogenomics and implications for precision medicine. Prog. Retin. Eye Res. 56, 58–83.

Gasiorowski, J.Z., Russell, P., 2009. Biological properties of trabecular meshwork cells. Exp. Eye Res. 88, 671–675.

Green, D.R., Galluzzi, L., Kroemer, G., 2014. Cell biology. Metabolic control of cell death. Science 345, 1250256.

He, Y., Leung, K.W., Zhang, Y.H., Duan, S., Zhong, X.F., Jiang, R.Z., Peng, Z., Tombran-Tink, J., Ge, J., 2008. Mitochondrial complex I defect induces ROS release and degeneration in trabecular meshwork cells of POAG patients: protection by antioxidants. Invest. Ophthalmol. Vis. Sci. 49, 1447–1458.

Izzotti, A., Sacca, S.C., Longobardi, M., Cartiglia, C., 2010. Mitochondrial damage in the trabecular meshwork of patients with glaucoma. Arch. Ophthalmol. 128, 724–730.

Keller, K.E., Bhattacharya, S.K., Borras, T., Brunner, T.M., Chansangpetch, S., Clark, A.F., Dismuke, W.M., Du, Y., Elliott, M.H., Ethier, C.R., Faralli, J.A., Freddo, T.F., Fuchshofer, R., Giovingo, M., Gong, H., Gonzalez, P., Huang, A., Johnstone, M.A., Kaufman, P.L., Kelley, M.J., Knepper, P.A., Kopczynski, C.C., Kuchtey, J.G., Kuchtey, R.W., Kuehn, M.H., Lieberman, R.L., Lin, S.C., Liton, P., Liu, Y., Lutjen-Drecoll, E., Mao, W., Masis-Solano, M., McDonnell, F., McDowell, C.M., Overby, D. R., Pattabiraman, P.P., Raghunathan, V.K., Rao, P.V., Rhee, D.J., Chowdhury, U.R., Russell, P., Samples, J.R., Schwartz, D., Stubbs, E.B., Tamm, E.R., Tan, J.C., Toris, C. B., Torrejon, K.Y., Vranka, J.A., Wirtz, M.K., Yorio, T., Zhang, J., Zode, G.S., Fautsch, M.P., Peters, D.M., Acott, T.S., Stamer, W.D., 2018. Consensus recommendations for trabecular meshwork cell isolation, characterization and culture. Exp. Eye Res. 171, 164–173.

Kwon, Y.H., Fingert, J.H., Kuehn, M.H., Alward, W.L., 2009. Primary open-angle glaucoma. N. Engl. J. Med. 360, 1113–1124.

Quigley, H.A., 2011. Glaucoma. Lancet 377, 1367–1377.

Roy Chowdhury, U., Hann, C.R., Stamer, W.D., Fautsch, M.P., 2015. Aqueous humor outflow: dynamics and disease. Invest. Ophthalmol. Vis. Sci. 56, 2993–3003.

Sacca, S.C., Pascotto, A., Camicione, P., Capris, P., Izzotti, A., 2005. Oxidative DNA damage in the human trabecular meshwork: clinical correlation in patients with primary open-angle glaucoma. Arch. Ophthalmol. 123, 458–463.

Sacca, S.C., Pulliero, A., Izzotti, A., 2015. The dysfunction of the trabecular meshwork during glaucoma course. J. Cell. Physiol. 230, 510–525.

Sakai, H., Shen, X., Koga, T., Park, B.C., Noskina, Y., Tibudan, M., Yue, B.Y., 2007. Mitochondrial association of myocilin, product of a glaucoma gene, in human trabecular meshwork cells. J. Cell. Physiol. 213, 775–784.

Sibayan, S.A., Latina, M.A., Sherwood, M.E., Flotte, T.J., White, K., 1998. Apoptosis and morphologic changes in drug-treated trabecular meshwork cells in vitro. Exp. Eye Res. 66, 521–529.

Stamer, W.D., Clark, A.F., 2017. The many faces of the trabecular meshwork cell. Exp. Eye Res. 158, 112–123.

Stothert, A.R., Fontaine, S.N., Sabbagh, J.J., Dickey, C.A., 2016. Targeting the ER-autophagy system in the trabecular meshwork to treat glaucoma. Exp. Eye Res. 144, 38–45.

Tamm, E.R., 2002. Myocilin and glaucoma: facts and ideas. Prog. Retin. Eye Res. 21, 395–428.

Tham, Y.C., Li, X., Wong, T.Y., Quigley, H.A., Aung, T., Cheng, C.Y., 2014. Global prevalence of glaucoma and projections of glaucoma burden through 2040: a systematic review and meta-analysis. Ophthalmology 121, 2081–2090.

Wang, S., Shi, X., Wei, S., Ma, D., Oyinlade, O., Lv, S.Q., Ying, M., Zhang, Y.A., Claypool, S.M., Watkins, P., Xia, S., 2018. Kruppel-like factor 4 (KLF4) induces mitochondrial fusion and increases spare respiratory capacity of human glioblastoma cells. J. Biol. Chem. 293, 6544–6555.

Wentz-Hunter, K., Ueda, J., Shimizu, N., Yue, B.Y., 2002. Myocilin is associated with mitochondria in human trabecular meshwork cells. J. Cell. Physiol. 190, 46–53.

Wordinger, R.J., Clark, A.F., 1999. Effects of glucocorticoids on the trabecular meshwork: towards a better understanding of glaucoma. Prog. Retin. Eye Res. 18, 629–667.

Xie, X., Akiyama, G., Bogarin, T., Saraswathy, S., Huang, A.S., 2019. Visual Assessment of Aqueous Humor Outflow. Asia Pac J Ophthalmol (Phila).

Yusoff, A.A.M., Abdullah, W.S.W., Khair, S., Radzak, S.M.A., 2019. A comprehensive overview of mitochondrial DNA 4977-bp deletion in cancer studies. Onco Rev. 13, 409.

Zeng, W., Wang, W., Wu, S., Zhu, X., Zheng, T., Chen, X., Ren, J., Gong, Y., Ke, M., 2020. Mitochondria and autophagy dysfunction in glucocorticoid-induced ocular hypertension/glaucoma mice model. Curr. Eye Res. 45, 190–198.

Zhang, J., Zhang, Q., 2019. Using Seahorse machine to measure OCR and ECAR in cancer cells, 1928 Methods Mol. Biol. 353–363.

1. Chowdhury, U. R., Madden, B. J., Charlesworth, M. C. & Fautsch, M. P. Proteome analysis of human aqueous humor. *Investig. Ophthalmol. Vis. Sci.* **51**, 4921–4931 (2010).

2. Chowdhury, U. R., Hann, C. R., Stamer, W. D. & Fautsch, M. P. Aqueous humor outflow: Dynamics and disease. *Investig. Ophthalmol. Vis. Sci.* **56**, 2993–3003 (2015).

3. Goel, M. Aqueous Humor Dynamics: A Review~!2010-03-03~!2010-06-17~!2010-09-02~! *Open Ophthalmol. J.* **4**, 52–59 (2010).

4. Brubaker, R. F. The flow of aqueous humor in the human eye. *Trans. Am. Ophthalmol. Soc.* **Vol. 80**, 391–474 (1982).

5. Civan, M. M. Chapter 1 Transport Components of Net Secretion of the Aqueous Humor and Their Integrated Regulation. *Curr. Top. Membr. Transp.* **45**, 1–24 (1997).

6. Robert, B. & Brown, E. B. Anatomy, Head and Neck, Eye Arteries. 1–14 (2004).

7. Johnson, M., McLaren, J. W. & Overby, D. R. Unconventional aqueous humor outflow: A review. *Exp. Eye Res.* **158**, 94–111 (2017).

8. Sunderland, D. K. & Sapra, A. Physiology, Aqueous Humor Circulation. *StatPearls* (2020).

9. Johnstone, M. A. The Aqueous Outflow System as a Mechanical Pump. *J. Glaucoma* **13**, 421–438 (2004).

10. Costagliola, C. *et al.* How many aqueous humor outflow pathways are there? *Surv. Ophthalmol.* **65**, 144–170 (2020).

11. Carreon, T., van der Merwe, E., Fellman, R. L., Johnstone, M. & Bhattacharya, S. K. Aqueous outflow - A continuum from trabecular meshwork to episcleral veins. *Prog. Retin. Eye Res.* **57**, 108–133 (2017).

12. Lam, K., Lawlor, M., Lam, K. & Lawlor, M. Anatomy of the Aqueous Outflow Drainage Pathways. *Minim. Invasive Glaucoma Surg.* 11–19 (2021). doi:10.1007/978-981-15-5632-6_2

13. Coca-Prados, M. & Escribano, J. New perspectives in aqueous humor secretion and in glaucoma: The ciliary body as a multifunctional neuroendocrine gland. *Prog. Retin. Eye Res.* **26**, 239–262 (2007).

14. Cvenkel, B. & Kolko, M. Current Medical Therapy and Future Trends in the Management of Glaucoma Treatment. *J. Ophthalmol.* **2020**, (2020).

15. Mertz, B. P. Intraocular Pressure. *Drug Discov. Eval. Pharmacol. Assay, Fourth Ed.* 3749–3752 (2015). doi:10.1007/978-3-319-05392-9_85

16. Bikuna-Izagirre, M. *et al.* Technological advances in ocular trabecular meshwork in vitro models for glaucoma research. *Biotechnol. Bioeng.* **119**, 2698–2714 (2022).

17. Keller, K. E. *et al.* Consensus recommendations for trabecular meshwork cell isolation, characterization and culture. *Exp. Eye Res.* **171**, 164–173 (2018).

18. Dismuke, W. M., Liang, J., Overby, D. R. & Stamer, W. D. Concentration-related effects of nitric oxide and endothelin-1 on human trabecular meshwork cell contractility. *Exp. Eye Res.* **120**, 28–35 (2014).

19. Wang, J., Liu, X. & Zhong, Y. Rho/Rho-associated kinase pathway in glaucoma (Review). *International Journal of Oncology* (2013). doi:10.3892/ijo.2013.2100

20. Tian, B., Gabelt, B. T., Geiger, B. & Kaufman, P. L. The role of the actomyosin system in regulating trabecular fluid outflow. *Exp. Eye Res.* **88**, 713–717 (2009).

21. Pattabiraman, P. P., Maddala, R. & Rao, P. V. Regulation of plasticity and fibrogenic activity of trabecular meshwork cells by rho GTPase signaling. *J. Cell. Physiol.* **229**, 927–

942 (2014).

22. Kieler, J. STUDIES ON HUMAN TRABECULAR CELLS PROPAGATED IN VITRO. *Cytotechnology* **2**, 8 (1989).

23. Grierson, I., Marshall, J., Robins, E. A Morphological Meshwork in Primary and Autoradiographic Culture : Study. *Exp Eye Res* **37**, 349–365 (1983).

24. Street, J. Preliminary Observations on Human Trabecular Meshwork Cells in vitro. *Ophthalmology* **3347**, 33–47 (1978).

25. ASHTON, N., BRINI, A. & SMITH, R. Anatomical studies of the trabecular meshwork of the normal human eye. *Br. J. Ophthalmol.* **40**, 257–282 (1956).

26. Alward, W. L. M., Longmuir, R. A. & Ophthalmology, A. A. of. *Color Atlas of Gonioscopy*. (American Academy of Ophthalmology, 2008).

27. Rohen, J. W., Schachtschabel, D. O., Lütjen-Drecoll, E., Rohrbach, M. & Berghoff, K. Morphological and Biochemical Studies on Cell and Tissue Cultures of Human Trabecular Meshwork. *Glaucoma Updat. II* 39–43 (1983). doi:10.1007/978-3-642-69096-9_8

28. Stamer, W. D., Seftor, R. E. B., Williams, S. K., Samaha, H. A. M. & Snyder, R. W. Isolation and culture of human trabecular meshwork cells by extracellular matrix digestion. *Curr. Eye Res.* **14**, 611–617 (1995).

29. Polansky, J. R., Wood, I. S., Maglio, M. T. & Alvarado, J. A. Trabecular Meshwork Cell Culture in Glaucoma Research: Evaluation of Biological Activity and Structural Properties of Human Trabecular Cells In Vitro. *Ophthalmology* **91**, 580–595 (1984).

30. Alvarado, J. A., Wood, I. & Polansky, J. R. Human trabecular cells Growth pattern and ultrastructural characteristics. 464–478 (2015).

31. Johnson, D. H. & Tschumper, R. C. The effect of organ culture on human trabecular meshwork. *Exp. Eye Res.* **49**, 113–127 (1989).

32. Tripathi, R. C. & Tripathi, B. J. Human trabecular endothelium, corneal endothelium, keratocytes, and scleral fibroblasts in primary cell culture. A comparative study of growth characteristics, morphology, and phagocytic activity by light and scanning electron microscopy. *Exp. Eye Res.* **35**, 611–624 (1982).

33. Hernandez, M. R. *et al.* Human trabecular meshwork cells in culture: Morphology and extracellular matrix components. *Investig. Ophthalmol. Vis. Sci.* **28**, 1655–1660 (1987).

34. J.W. Rohen 1, D. O. S. 2 and R. W. 1. Structural Changes of Human and Monkey Trabecular Meshwork Following in vitro Cultivation. *Clin. Exp. Ophthalmol.* **229**, 265–270 (1982).

35. Grierson, I. & Rahi, A. H. S. Microfilaments in the cells of the human trabecular meshwork. *Br. J. Ophthalmol.* **63**, 3–8 (1979).

36. Grierson, I. *et al.* Graefe ' s Archive Ophthalmology and their synthetic activities. *Clin. Exp. Ophthalmol.* (1985).

37. Stamer, W. D. & Clark, A. F. The many faces of the trabecular meshwork cell. *Exp. Eye Res.* **158**, 112–123 (2017).

38. Gasiorowski, J. Z. & Russell, P. Biological properties of trabecular meshwork cells. *Exp. Eye Res.* **88**, 671–675 (2009).

39. De Kater, A. W., Spurr-Michaud, S. J. & Gipson, I. K. Localization of smooth muscle myosin-containing cells in the aqueous outflow pathway. *Investig. Ophthalmol. Vis. Sci.* **31**, 347–353 (1990).

40. De Kater, A. W., Shahsafaei, A. & Epstein, D. L. Localization of smooth muscle and

nonmuscle actin isoforms in the human aqueous outflow pathway. *Investig. Ophthalmol. Vis. Sci.* **33**, 424–429 (1992).

41. Comes, N., Buie, L. K. K. & Borrás, T. Evidence for a role of angiopoietin-like 7 (ANGPTL7) in extracellular matrix formation of the human trabecular meshwork: Implications for glaucoma. *Genes to Cells* **16**, 243–259 (2011).

42. Tomarev, S. I., Wistow, G., Raymond, V., Dubois, S. & Malyukova, I. Gene expression profile of the human trabecular meshwork: NEIBank sequence tag analysis. *Investig. Ophthalmol. Vis. Sci.* **44**, 2588–2596 (2003).

43. Gonzalez, P., Epstein, D. L. & Borras, T. Characterization of gene expression in human trabecular meshwork using single-pass sequencing of 1060 clones. *Investig. Ophthalmol. Vis. Sci.* **41**, 3678–3693 (2000).

44. Patel, G. *et al.* Molecular taxonomy of human ocular outflow tissues defined by single-cell transcriptomics. *Proc. Natl. Acad. Sci. U. S. A.* **117**, 12856–12867 (2020).

45. van Zyl, T. *et al.* Cell atlas of aqueous humor outflow pathways in eyes of humans and four model species provides insight into glaucoma pathogenesis. *Proc. Natl. Acad. Sci. U. S. A.* **117**, 10339–10349 (2020).

46. Liton, P. B., Luna, C., Challa, P., Epstein, D. L. & Gonzalez, P. Genome-wide expression profile of human trabecular meshwork cultured cells, nonglaucomatous and primary open angle glaucoma tissue. *Mol. Vis.* **12**, 774–790 (2006).

47. Chang, I. L. *et al.* Expression of modified low-density lipoprotein receptors by trabecular meshwork cells. *Curr. Eye Res.* **10**, 1101–1112 (1991).

48. Stone, E. M. *et al.* Identification of a gene that causes primary open angle glaucoma. *Science (80-.).* **275**, 668–670 (1997).

49. Kubota, R. *et al.* A novel myosin-like protein (myocilin) expressed in the connecting cilium of the photoreceptor: Molecular cloning, tissue expression, and chromosomal mapping. *Genomics* **41**, 360–369 (1997).

50. J R Polansky 1, D J Fauss, P Chen, H Chen, E Lütjen-Drecoll, D Johnson, R M Kurtz, Z D Ma, E Bloom, T. D. N. Cellular Pharmacology and Molecular Biology of the Trabecular Meshwork Inducible Glucocorticoid Response Gene Product. 1–14 (2004).

51. Tseng, P., Pushkarsky, I. & Di Carlo, D. Metallization and biopatterning on ultra-flexible substrates via dextran sacrificial layers. *PLoS One* **9**, (2014).

52. De Ieso, M. L., Kuhn, M., Bernatchez, P., Elliott, M. H. & Stamer, W. D. A Role of Caveolae in Trabecular Meshwork Mechanosensing and Contractile Tone. *Front. Cell Dev. Biol.* **10**, 1–20 (2022).

53. Murphy, C. G., Yun, A. J., Newsome, D. A. & Alvarado, J. A. Localization of extracellular proteins of the human trabecular meshwork by indirect immunofluorescence. *Am. J. Ophthalmol.* **104**, 33–43 (1987).